

A Review of Different Models Derived from Classical Kolmogorov, Johnson and Mehl, and Avrami (KJMA) Theory to Recover Physical Meaning in Solid-State Transformations

Javier S. Blázquez,* Francisco J. Romero, Clara F. Conde, and Alejandro Conde

The classical theory of solid-state transformation based on nucleation and growth processes, developed by Kolmogorov, Johnson and Mehl, and Avrami (KJMA theory), is widely used in many different fields of research. In KJMA theory, two parameters (the frequency factor and, particularly, the Avrami exponent) can supply information about the mechanisms involved in the transformation. Despite its apparent simplicity, on the one hand, the results derived from this theory can be strongly affected by the indetermination of experimental data (e.g., onset of the transformation). On the other hand, KJMA theory is developed for isothermal polymorphic transformations in which randomly distributed nuclei grow in convex shapes. However, several procedures have extended KJMA theory to nonisothermal regimes and to many different processes deviating from those premises. Herein, the requirements of KJMA theory and the expected deviations for these approximations are briefly discussed. In addition, some strategies are proposed for recovering physical meaning from the effective parameters deduced in several transformations including nanocrystallization and martensitic transformations for which results can be interpreted under the approximation of instantaneous growth.

Johnson and Mehl,^[2] and Avrami^[3] (KJMA or JMAK) equation

$$X = 1 - \exp(-K \cdot (t - t_0)^n) \quad (1)$$

where X is the transformed fraction, K is a prefactor (in order to consider a dimensionally correct frequency factor, $K = k^n$ can be used instead), t_0 is the induction time, and n is the Avrami exponent. Kinetic data are generally analyzed in the frame of Equation (1) using the so-called KJMA-plot which represents $\ln(-\ln(1 - X))$ as a function of $\ln(t - t_0)$. The slope of KJMA-plot is the Avrami exponent.

It is worth mentioning that Equation (1) can be obtained after the useful definition of the extended transformed volume, X^* . This magnitude corresponds to the fraction transformed but neglecting the overlapping between growing regions. On the one hand, X^* has no direct physical meaning as it reaches values above 1 and, in fact, it never saturates. On the other hand, X^* can be easily calculated when the nucleation and growth laws are known.

and growth laws are known.

In 1937, Kolmogorov mathematically developed the following equation correlating the actual and the extended transformed fractions for transformations in which randomly distributed nuclei geometrically compete for the available space in the formation of a new product phase.^[4]

$$X = 1 - \exp(-X^*) \quad (2)$$


Kolmogorov found Equation (1) as a particular solution to Equation (2) in two cases^[4]: 1) constant nucleation rate and constant linear growth rate (with $n = 4$); 2) instantaneous nucleation and constant linear growth rate (with $n = 3$).

Independently from Kolmogorov, in 1939 Johnson and Mehl were able to describe the pearlite formation from austenite by using Equation (1) with $n = 4$.^[2] From then, and soon later further developed by Avrami, KJMA theory has been widely used in materials science^[5–9] and in many other fields of research including chemical reactions,^[10–14] medicine,^[15–17] biology,^[18–22] genetics,^[23–25] food research,^[26–30] sociology,^[31] etc. **Figure 1** shows the distribution of research works containing “Avrami” in the different subject areas and years since 1960.

1. Introduction

The classical KJMA theory of transformation in solid state assumes nucleation and growth processes which consider the geometrical impingement between different growing regions. This idea is summarized in the well-known Kolmogorov,^[1]

J. S. Blázquez, F. J. Romero, C. F. Conde, A. Conde
Dpto. Física de la Materia Condensada
ICMSE-CSIC
Universidad de Sevilla
P.O. Box 1065, 41080 Sevilla, Spain
E-mail: jsebas@us.es

 The ORCID identification number(s) for the author(s) of this article can be found under <https://doi.org/10.1002/pssb.202100524>.

© 2022 The Authors. physica status solidi (b) basic solid state physics published by Wiley-VCH GmbH. This is an open access article under the terms of the Creative Commons Attribution-NonCommercial-NoDerivs License, which permits use and distribution in any medium, provided the original work is properly cited, the use is non-commercial and no modifications or adaptations are made.

DOI: 10.1002/pssb.202100524

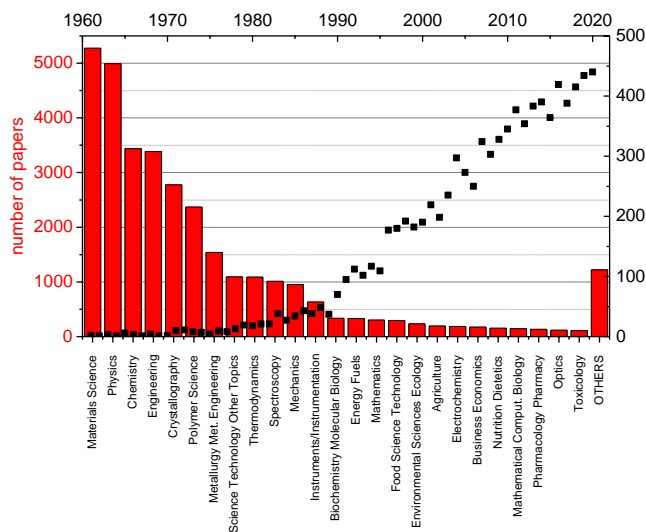


Figure 1. Distribution of research papers containing “Avrami” as a function of the area of research (bars, left axis) and year of publication (symbols, right axis). Data obtained from Web of Science (September 20, 2021).

Therefore, the use of KJMA analysis has been extended beyond its rigorous limits. However, despite this lack of rigor, deviations from KJMA requisites can be negligible allowing for an effective interpretation of the mechanisms involved in the transformation process. The aim of the present article is to show some examples in which an effective KJMA analysis still preserves some physical information of the transformation process, although the strict conditions are somehow not fulfilled.

The article is structured as follows: Section 1 presents KJMA equation and its wide use in a broad range of scientific areas. In the next section, the requisites of KJMA equation, summarized in the five postulates of Kolmogorov as collected by Burbelko et al.,^[4] are briefly described and negligibility of certain deviations is discussed. Section 3 shortly describes the development of the extended transformed fraction from known laws of nucleation and growth. Section 4 describes the important role of accurate determination of experimental data such as the induction time and the final transformed fraction even for ideal KJMA processes. Section 5 reviews some extensions of KJMA theory to nonisothermal regimes. Melting of pure In is described as an example. Section 6 describes some of our proposed strategies to afford the results from effective KJMA analysis applied to systems for which deviations from some of the postulates of Kolmogorov are no longer negligible. Some simple simulations are performed to evaluate the importance of deviations of ideal systems from the strict requirements of KJMA theory, including diffusion controlled growth and instantaneous growth approximation. Crystallization of amorphous alloys, mechanical amorphization of ball-milled powders, and martensitic transformation are described as examples. Finally, some conclusions are briefly summarized.

2. Requirements to Obtain the KJMA Equation

Burbelko et al.^[4] summarized the requisites for KJMA theory to be valid in the five postulates of Kolmogorov: 1) The initial parent

phase is progressively and completely replaced by a product phase. 2) The volume of any transformed region is tiny with respect to the whole volume of the system. 3) Nucleation is random. 4) The shape of the growing phase is convex. 5) The linear growth rate can be expressed as a product of a time-dependent function and a direction-dependent function.

To require a progressive and complete replacement of the initial phase by the product phase would restrict the use of KJMA theory to none but polymorphic transformations. However, KJMA theory is broadly applied beyond this limit as we will show in Section 6. Postulates number 2 and 3 are not very restrictive. In the first case, we are considering the formation of polycrystalline systems and assuming an infinite limit for the space to be transformed in comparison with the size of an individual crystal. In the third postulate, we are not restricted to homogeneous nucleation but the heterogeneous nucleation centers (defects, grain boundaries, etc.) must be randomly distributed.

Concerning postulates number 4 and 5, they can be reformulated following the requisites appearing in the review article from Korobov^[32] on KJMA theory in which it is pointed that all nuclei must have a common shape and orientation, and that the growth rate of a nucleus must not depend on its growing time. Both conditions prevent overestimation of transformed fraction avoiding the overgrowth contribution from phantom nuclei, which are those contributing to X^* but formed in an already transformed region. When these requisites are fulfilled, all the contribution to the extended volume corresponding to the growth of a phantom nucleus will overlap with the already transformed region of the parent crystal where the phantom nucleus appears. Therefore, KJMA equation is valid to describe the actual transformed fraction.

However, when linear growth rate decreases with the growing time, a phantom nucleus (close enough to the interface of the transformed region into which it appeared) can overcome the limit of this transformed region as the boundary of the former moves faster than the latter, leading to an overgrowth region (see Figure 2a). This is the case of diffusion controlled growth, for which the linear growth rate of a crystal decreases with the growing time as $\propto (t - \tau)^{-0.5}$, where t is the observation time and τ is the nucleation time. In Section 6, we will show some simple simulations to account for the importance of the effect of overgrowth regions.

Moreover, when anisotropic growth occurs and orientation is not the same for all the crystallites, nonoverlapped regions of the extended transformed fractions can be physically banned (schematic representations can be found in Figure 2b,c).

These problems were afforded in two dimensions by Tomellini and Fanfoni^[33] calculating the fraction transformed without the contribution of the phantom nuclei. On the other hand, Kooi,^[34] using Monte Carlo simulations, modifies the extended transformed fraction and finds the time at which the transformation deviates from normal KJMA to a blocking regime in systems for which dimensionality of growth is smaller than that of the corresponding space.

3. Development of KJMA Equation

Extended transformed fraction, X^* , can be easily calculated after adding the expected volume of each transformed region

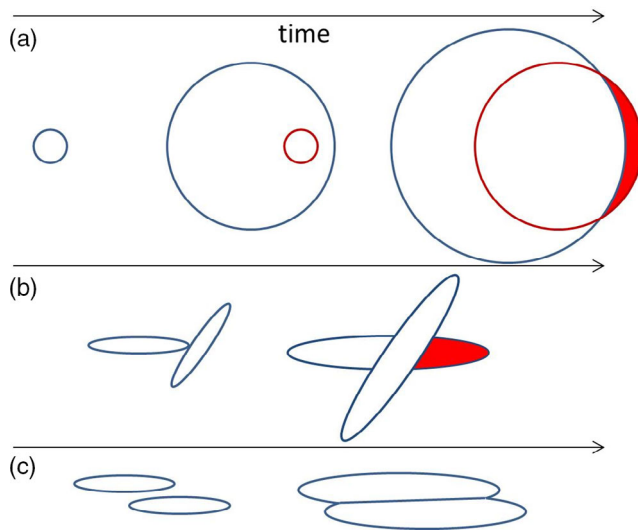


Figure 2. Schematic pictures showing that: a) decreasing growth rate with growing time, as it occurs in diffusion controlled processes, may lead to the appearing of overgrowth regions (red area). b) Anisotropic growth can also lead to overgrowth regions when orientation and shape is not shared by all the crystallites.^[7,32,34] c) When orientation and shape are the same for all the crystallites, overgrowth does not occur.

whether it was nucleated at a certain time or it existed before the transformation started

$$X^*(t) = \int_0^t I(\tau) V(\tau, t) d\tau + \int_0^\infty \frac{dN_0}{dr_0} V(r_0, t) dr_0 \quad (3)$$

The first integral depends on the nucleation rate per unit volume $I(t) = dN(t)/dt$ (being $N(t)$ the number of nuclei per unit volume) and corresponds to the contribution to $X^*(t)$ at the observation time t of those regions nucleated at time τ ($0 < \tau < t$) which should have grown (neglecting any impingement) to a volume

$$V(\tau, t) = \frac{4\pi}{3} \left[r^*(\tau) + \int_\tau^t u(t', T) dt' \right]^3 \quad (4)$$

For simplicity, spherical regions are assumed and $r^* = \frac{2\gamma_{SL} T_E}{\Delta T \cdot \Delta H}$ is the critical radius for a nucleus to be stable,^[35,36] with γ_{SL} is the surface energy, T_E is the equilibrium temperature between the initial and final phases, $\Delta T = T - T_E$ is the thermal span from the equilibrium temperature, and ΔH is the latent heat ascribed to the transformation. Moreover, $u(t', T)$ is the linear growth rate at time t' and depends on temperature T .

The second integral corresponds to the contribution to $X^*(t)$ of the growth of dN_0 preexisting regions per unit volume of the product phases, with an initial radius between r_0 and $r_0 + dr_0$, to a volume: $V(r_0, t)$.

$$V(r_0, t) = \frac{4\pi}{3} \left[r_0 + \int_\tau^t u(t', T) dt' \right]^3 \quad (5)$$

Equation (4) and (5) are valid for spherical crystals and, in general, the size of the nuclei is small enough and can be neglected. KJMA theory is a global theory of the transformation and many characteristics of growth processes (e.g., cooperative movement of atoms in coherent interfaces) are overseen in the KJMA model. However, anisotropic growth can be considered but, as described above, is only valid when shape and orientation are the same for all the crystals, preventing overgrowth regions.^[7,32,34] For example, particularizing to an ellipsoidal crystal, in the case of Equation (4)

$$V(\tau, t) = \frac{4\pi}{3} \left[\int_\tau^t u_x(t', T) dt' \right] \left[\int_\tau^t u_y(t', T) dt' \right] \left[\int_\tau^t u_z(t', T) dt' \right] \quad (6A)$$

where u_x , u_y , and u_z are the linear growth on the corresponding axes of the ellipsoid that should be common for all crystallites. A general approach is to consider absence of growth in one or two dimensions to represent the formation of needle-like crystals (1D growth) or platelets (2D growth). Several authors have studied this limitation in the growth dimensionality. Kooi^[34] using Monte Carlo simulations studied the formation of 1D crystals in 2D and 3D spaces, founding that KJMA describes the process at the initial state of the transformation. In that article, a well-defined transition time was obtained after which the transformation progresses in a blocking regime. Following the interpretation of Korobov,^[32] and assuming that the shape and orientation of the crystals are common, Equation (6A) can be approached to

$$V(\tau, t) = \frac{\pi}{4} D^2 \left[\int_\tau^t u(t', T) dt' \right]^2 \quad (6B)$$

for needle-like crystals of diameter D , and

$$V(\tau, t) = \pi \lambda \left[\int_\tau^t u(t', T) dt' \right]^2 \quad (6C)$$

for thin discs of thickness λ .

Similar equations could be obtained for $V(r_0, t)$, neglecting the initial radius of those preexisting regions.

Therefore, Equation (3) can be explicitly stated as

$$X^*(t) = \int_0^t I(\tau) C_1 \left[\int_\tau^t u(t', T) dt' \right]^{d_1} d\tau + N_0 C_0 \left[\int_\tau^t u(t', T) dt' \right]^{d_0} \quad (7)$$

where d_1 and d_0 are the dimension of growth for the new nucleated regions and for the preexisting ones, respectively,

and C_I and C_0 are geometrical factors with dimension of length at the power $(3 - d_I)$ and $(3 - d_0)$, respectively.

Concerning nucleation phenomenon, two simple cases already analyzed by Kolmogorov are considered when analyzing in the frame of KJMA theory.

On the one hand, assuming constant nucleation rate, neglecting the presence of already transformed regions, Equation (7) becomes

$$X^*(t) = I(T) \int_0^t C_I \left[\int_{\tau}^t u(t', T) dt' \right]^{d_I} d\tau \quad (8)$$

but only in the case of isothermal conditions, as nucleation rate, and generally the transformation rate,^[37] strongly depends on temperature following an Arrhenius law

$$I(T) = I_0 \exp\left(-\frac{(Q+W)}{k_B T}\right) \quad (9)$$

where Q is the activation energy for an atom to be incorporated to the new phase and W is the work needed to form a stable nucleus.^[35]

On the other hand, in the case of neglecting the formation of new nuclei and assuming that the transformation is only due to the growth of preexisting nuclei, the second addition term in Equation (7) is the only one to be considered.

Concerning growth phenomena, analysis in the frame of KJMA theory considers two extreme cases: interface controlled growth, when diffusion of heat and atoms is fast enough compared to the time required for an atom to jump into the product phase; and diffusion controlled growth, when the progress of the transformation is governed by this mechanism. The latter mechanism, as described above, is not strictly valid in KJMA frame as it leads to overgrowth of phantom nuclei (see Figure 2a). In fact, KJMA theory accounts for the phantom nuclei but when linear growth decreases as the crystal grows (as it occurs in diffusion controlled growth) this implies that a phantom nucleus, which is formed inside an already transformed region, grows faster than its host region, and can go beyond its limit. We will show in Section 6 that deviations due to this overgrowth are expected to be negligible and, in agreement with other authors,^[38,39] KJMA theory can be used as a fair approach to describe diffusion controlled growth processes.

On the one hand, assuming an interface controlled growth leads to time independent linear growth rate $u(T)$, which implies a volume of the growing particle

$$V(\tau, t) = C_I \left[\int_{\tau}^t u(T) dt' \right]^d = K_1(T)(t - \tau)^d \quad (10)$$

As the linear growth rate depends on temperature, only for isothermal transformations it should be properly written the final identity with $K_1(T) = C_I [u(T)]^d$. An Arrhenius law can be approximated to the linear growth in the case of interface controlled growth^[37]

$$u(T) = u_0 \exp\left(-\frac{Q}{k_B T}\right) \quad (11)$$

which is constant for a constant temperature.

On the other hand, a diffusion controlled growth is characterized by a linear growth rate that depends on the observed time, t , the time the nucleus was formed, τ , and the temperature, T

$$u(T, t, \tau) = \sqrt{\frac{2D(T)}{(t - \tau)}} \quad (12)$$

where $D(T)$ is the diffusion coefficient, and the volume of the growing particle (in isothermal conditions) would be

$$V(\tau, t) = C_I \left[\int_{\tau}^t \sqrt{\frac{2D(T)}{t' - \tau}} dt' \right]^d = K_2(T)(t - \tau)^{d/2} \quad (13)$$

In this case, the temperature-dependent prefactor is $K_2(T) = 2C_I \sqrt{2D(T)}$, with an Arrhenius law describing the temperature dependence of the diffusion coefficient.

Therefore, in isothermal conditions and taking into account the different possibilities described above, the extended volume fraction can be expressed as

$$X^*(t) = K(T)(t - t_0)^n \quad (14)$$

where Avrami exponent $n = n_I + d \cdot n_G$, with $n_I = 1$ for constant nucleation process or $n_I = 0$ for absence of nucleation, and $n_G = 1$ for interface controlled growth or $n_G = 0.5$ for diffusion controlled growth. Restricted possibilities with physical meaning ($0.5 \leq n \leq 4$) are collected in Table 1. As it is observed in this table, ambiguity can be found for some values of n and,

Table 1. Possible physical meaningful values of Avrami exponent n in the frame of KJMA theory.

Avrami exponent n	Nucleation exponent n_I	Growth exponent n_G	Dimension of growth d
0.5	No nucleation	Diffusion controlled	1
1	Constant nucleation rate	No growth	0
	No nucleation	Interface controlled	1
1.5	No nucleation	Diffusion controlled	2
	Constant nucleation rate	Diffusion controlled ^{a)}	1
2	No nucleation	Diffusion controlled	3
	Constant nucleation rate	Interface controlled	1
2.5	Constant nucleation rate	Diffusion controlled ^{a)}	2
	No nucleation	Interface controlled	2
3	Constant nucleation rate	Diffusion controlled ^{a)}	3
	No nucleation	Interface controlled	2
4	Constant nucleation rate	Interface controlled	3
	No nucleation	Interface controlled	3

^{a)}Diffusion controlled processes for which nucleation is extended along the transformation are affected by overgrowth of phantom nuclei. The Avrami exponent would correspond to a maximum limit when this overgrowth is negligible.

therefore, it is important to combine this kinetic analysis with microstructural observations to elucidate which are the mechanisms involved in the transformation.

In a semiquantitative way, values of $n_f < 1$ are ascribed to a decreasing nucleation rate and $n_f > 1$ to an increasing nucleation rate. This can be implemented in Equation (7) assuming a power expression for the number of nuclei as a function of time,^[34] leading to a nucleation rate of the form: $I(t) = t^a$ with $-1 < a < 0$ for a decreasing nucleation rate process and $a > 0$ for an increasing nucleation rate process.

The relationship between actual transformed fraction, X , and the extended one, X^* , is obtained statistically as^[40]

$$\frac{dX}{dX^*} = (1 - X)^\eta \quad (15)$$

In KJMA theory, the impingement exponent $\eta = 1$ but other kinetic theories are developed assuming a stronger impingement exponent. For example, Austin–Rickett model^[41] can be developed using $\eta = 2$. Tagami and Tanaka^[42] proposed an intermediate value of η defining the overlap factor $\gamma = 2 - \eta$ to describe nucleation and halt in growth processes. These are processes in which the crystals grow to a fixed size. The overlap factor was developed to account for the phantom crystals from phantom nuclei which should be accounted in X^* . The value of $\gamma = 0.75$ corresponds to needle-like crystals, $\gamma = 0.5865$ to planar disc-like crystals, and $\gamma = 0.48675$ to spherical crystals. Starink^[40] also proposed a variable impingement parameter to approximate several deviations from KJMA requirements.

The relation $dX/dX^* = (1 - X)$ between the extended and actual transformed fractions described by Equation (15) with $\eta = 1$ was obtained mathematically by Kolmogorov under rigorous requirements (as we qualitatively collected in Section 2). However, as an approximation, it can be understood as the simplest relation between two magnitudes being equal when they are close to zero but describing the saturation behavior of X at 1 whereas X^* never saturates. This may explain why KJMA kinetics is a fairly good approximation even when the systems depart from its strict requirements and why different kinetic approaches lead to similar equations to KJMA one.^[32]

Integration of Equation (15) leads to

$$\int_0^X \frac{dX}{(1 - X)^\eta} = \int_0^{X^*} dX^* \rightarrow \begin{cases} \eta = 1 \rightarrow -\ln(1 - X) = X^* \\ \eta \neq 1 \rightarrow \frac{1 - (1 - X)^{1-\eta}}{1-\eta} = X^* \end{cases} \quad (16)$$

Substitution of Equation (14) in (16) for $\eta = 1$ leads to Equation (1). Therefore, experimentally, we will consider the value of $-\ln(1 - X) = X^*$ and, in the following, we will discuss on the deviations of the different models from theoretical X^* . Therefore, the KJMA-plot represents $\ln(-\ln(1 - X)) = \ln(X^*)$ versus $\ln(t - t_0)$.

4. Effects of Indetermination of Experimental Data in KJMA Analysis

4.1. Effects of Indetermination in the Induction Time

In order to apply Equation (1), we need to obtain experimental data on transformed fraction X as a function of the time of transformation t . In this sense it is very important to take into account that we also need an accurate estimation of the induction time, t_0 .

As we will see below, a wrong estimation of the induction time leads to important deviation effects. **Figure 3** shows how the effective Avrami exponent becomes reduced when experimental t_0 delays with respect to the theoretical value at which the transformation starts (i.e., $X(t_0) = 0$ but we normally detect the onset once the magnitude we use to follow transformation appreciably changes from its baseline value). It is particularly important to notice that the steepest slope method to obtain the onset, which is widely used, supplies a correct value only for $n = 1$.

The induction time measured from steepest slope method, t_{slope} , can be obtained as a function of Avrami exponent for theoretical curves, taking into account that the time at which the transformation rate is maximum corresponds to $t_{\text{inf}} = \frac{1}{k} \left(\frac{n-1}{n}\right)^{1/n}$:

$$t_{\text{slope}} = t_{\text{inf}} - \frac{X(t_{\text{inf}})}{\frac{dX(t_{\text{inf}})}{dt}} \quad (17)$$

Results are shown in **Figure 4** for the different values of n along with the transformed fractions at this induction time $X(t_{\text{slope}})$, which can be $\approx 10\%$ for high values of n . Taking into account theoretical results from Figure 3 and 4, it is important to know that this effect can lead to erroneous values. Definitely, the steepest slope method is only valid when $n = 1$. However, we can estimate the correct induction time, t_0 , from the proportionality shown in Figure 4c between time spans: $\alpha = \frac{(t_{\text{slope}} - t_0)}{(t_{\text{inf}} - t_{\text{slope}})}$, which linearly depends on Avrami exponent: $\alpha = (-0.578 \pm 0.009) + (0.564 \pm 0.03)n$. Therefore, the correct induction time can be

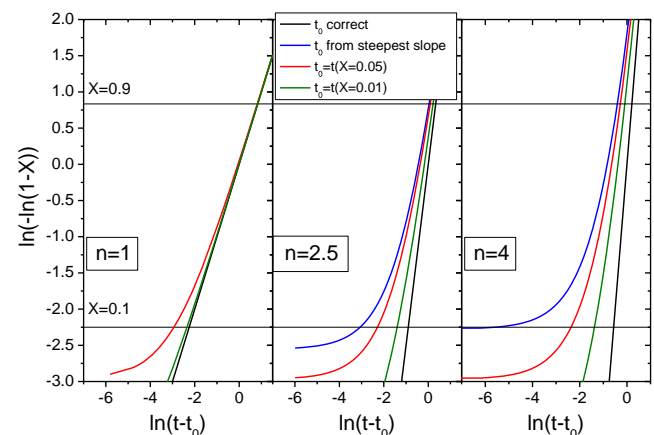


Figure 3. Effect of indetermination of induction time on the KJMA-plot for three different values of the Avrami exponent. Limit values corresponding to $X = 0.1$ and $X = 0.9$ are shown as horizontal lines.

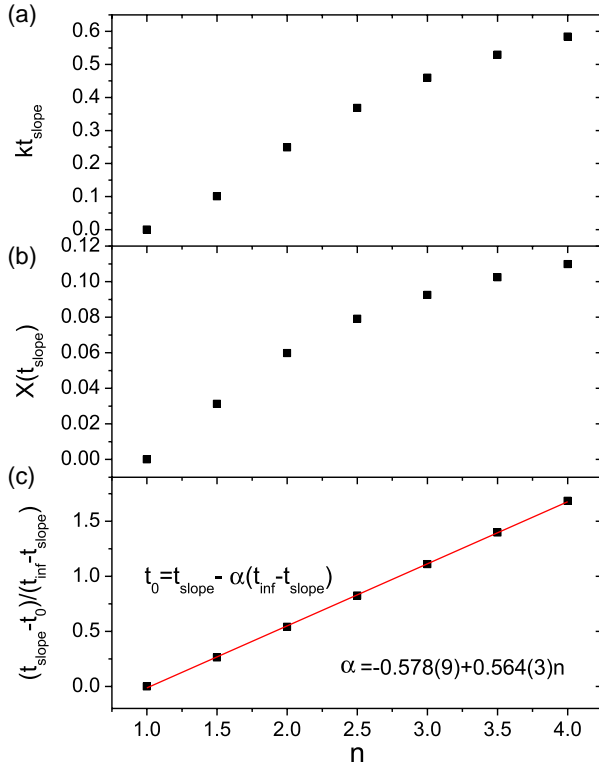


Figure 4. Variation with the Avrami exponent of a) the onset of the transformation estimated from the steepest slope method, t_{slope} , b) the transformed fraction at this time, and c) the ratio between $(t_{\text{slope}} - t_0)$ and $(t_{\text{inf}} - t_{\text{slope}})$ spans.

obtained as

$$t_0 = t_{\text{slope}} - \alpha(t_{\text{inf}} - t_{\text{slope}}) \quad (18)$$

Something similar would be obtained when applying the steepest slope method to determine the induction time (or more generally, the onset of the transformation) using dX/dt curves. In such a case, the value obtained from steepest slope is generally used as the calibration onset temperature in differential scanning calorimetry.

Although KJMA assumes simple processes with constant kinetic parameters through the transformation, complexities of the actual process can be better evidenced by obtaining the so-called local Avrami exponent, first proposed by Calka and Radlinski:^[43]

$$n(X) = \frac{d \ln(-\ln(1-X))}{d \ln(t-t_0)} \quad (19)$$

Figure 5 shows how the effective local Avrami exponent deviates from the theoretical values due to a wrong determination of t_0 . Qualitatively, it is observed that overestimation of t_0 leads to an underestimation of n and vice versa. This behavior could be used to detect errors in the determination of the onset of simple transformations. In the case of $n = 1$, deviations are almost negligible for $X > 0.2$.

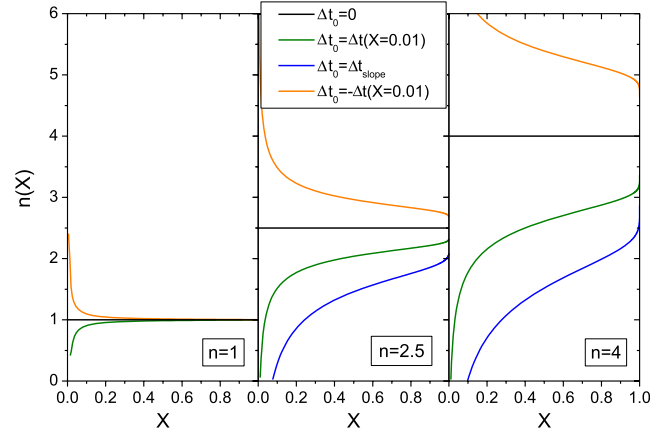


Figure 5. Effect of the indetermination of the induction time on the effective local Avrami exponents for different values of n .

4.2. Effects of Indetermination in the Final Transformed Fraction in Nonpolymorphic Transformations

Although first postulate of Kolmogorov assumes a complete transformation of the system, this restriction is generally overseen after normalizing the transformed fraction to 1 at the end of the considered process by dividing the actual transformed fraction $x(t)$ by the final one, $X = x(t)/x^{\text{end}}$. In fact, KJMA analysis was widely applied to primary crystallization,^[44–51] precipitation,^[52–58] eutectoid,^[59,60] and quasicrystals formation^[61] using this normalization. This yields an extra source of error in the data, as the final transformed fraction must be measured. **Figure 6** shows the effect of indetermination in the final transformed fraction x^{end} .

Underestimating the final transformed fraction is not seriously affecting n but at very high values of X . However, overestimation can lead to two slopes artifact but n can be obtained from the linear part (for such a high value as 30% overestimation, Avrami exponent only changes $\approx 10\%$). In any

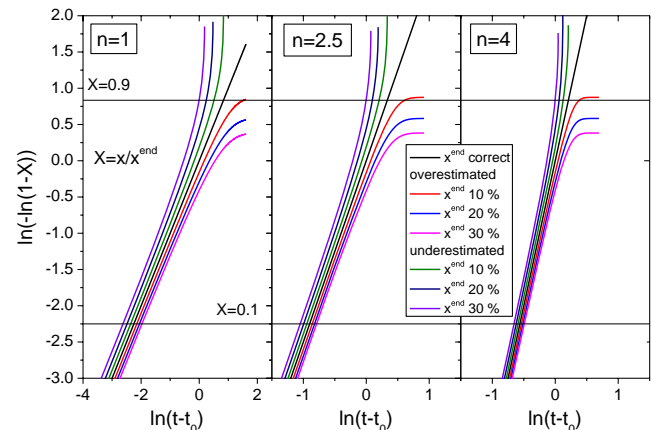


Figure 6. Effect of indetermination in the final transformed fraction on KJMA-plots for different values of n . Limit values corresponding to $X = 0.1$ and $X = 0.9$ are shown as horizontal lines.

case, it is important to be aware of using X data in a correct range, avoiding the extreme values.

When compositions of initial and final phases are not the same, a side effect can be derived from the compositional change of the environment of the growing crystal. This may affect the growth rate and even lead to soft impingement,^[39,40,51,62,63] which is generally used to distinguish between the pure geometrical impingement considered in KJMA and that produced by the overlapping of concentration gradients.

5. Extensions of KJMA Theory to Nonisothermal Conditions

As described above, KJMA theory is strictly valid for isothermal conditions. However, the advantages of constant heating rate experiments^[37] made the extension of KJMA to nonisothermal regimes a desired goal since earlier times.^[5,6,64–68] In this section, we will briefly discuss on the consequences of a constant heating rate regime for a hypothetical process following KJMA kinetics.

We will consider the case with no preexistent regions (no quenched in nuclei) in nonisothermal conditions. In this case, neither $I(T)$ nor $u(t', T)$ can be extracted from the integral in Equation (7) and thus, for nonisothermal cases, using Equation (8), (11), and (12), it is possible to write

$$X^*(T) = C_I I_0 \int_0^t \exp\left(-\frac{Q_I}{k_B T}\right) \left[\int_\tau^t u_0 \exp\left(-\frac{Q_G}{k_B T}\right) dt' \right]^d d\tau \quad (20A)$$

for interface controlled growth, and

$$X^*(T) = C_I I_0 \int_0^t \exp\left(-\frac{Q_I}{k_B T}\right) \left[\int_\tau^t \sqrt{\frac{2D_0}{(t' - \tau)}} \exp\left(-\frac{Q_G}{k_B T}\right) dt' \right]^d dt \quad (20B)$$

for diffusion controlled growth. In both cases we will assume that I_0 , D_0 , and u_0 as well as the activation energies do not change during the transformation due to, for example, neglected temperature dependence in our approximations, compositional changes of the matrix, or activation of new mechanisms of nucleation.

Assuming a constant heating/cooling rate $\beta = dT/dt$, some further simplification can be obtained:

$$X^*(T) = C_I I_0 u_0^d \int_{T_0}^T \exp\left(-\frac{Q_I}{k_B \theta}\right) \left[\int_\theta^T \exp\left(-\frac{Q_G}{k_B T'}\right) \frac{dT'}{\beta} \right]^d \frac{d\theta}{\beta} \quad (21A)$$

for interface controlled growth, and

$$X^*(T) = C_I I_0 (2D_0)^{\frac{d}{2}} \int_{T_0}^T \exp\left(-\frac{Q_I}{k_B \theta}\right) \left[\int_\theta^T \sqrt{\frac{1}{(T' - \theta)}} \exp\left(-\frac{Q_G}{k_B T'}\right) \frac{dT'}{\beta^{0.5}} \right]^d \frac{d\theta}{\beta} \quad (21B)$$

for diffusion controlled growth (neglecting overgrowth of phantom nuclei). We can have a more general equation to describe both cases and taking out of the integral the heating rate dependency

$$X^*(T) = \frac{C}{\beta^{d \cdot n_G + 1}} \int_{T_0}^T \exp\left(-\frac{Q_I}{k_B \theta}\right) \left[\int_\theta^T (T' - \theta)^{n_G - 1} \exp\left(-\frac{Q_G}{k_B T'}\right) dT' \right]^d d\theta \quad (22)$$

which can be simplified to

$$X^*(T) = \frac{Z(T, T_0)}{\beta^{d \cdot n_G + 1}} \quad (23)$$

where $Z(T, T_0)$ is the crystallization function. Ozawa^[64] proposed a method in which, for a fixed temperature, a plot of $\ln(-\ln(1 - X))$ versus $-\ln(\beta)$ might supply a straight line with the Avrami exponent as the slope. However, Ozawa's method implicitly assumes that all the kinetic parameters are constant along the transformation process, as the transformation is compared at different stages of the transformation (i.e., for a given temperature, $Z(T, T_0)$ is independent of X or β). Although this is apparently consistent with KJMA theory, it prevents any analysis on the local Avrami exponent and neglects any effect of T_0 .

Ozawa's method was applied in the present study to the melting of an indium sample used as standard for calibration of the differential scanning calorimeter (Perkin-Elmer DSC7). This equipment has two independent furnaces which supply heat to the sample and the reference, respectively, to keep them at the same temperature. This minimizes the errors due to differences in temperatures^[37] between reference and sample in other thermal analyzers. The mass of the sample was 21.65 mg and it was heated at heating rates between 5 and 80 K min⁻¹ (Figure 7a) after correcting the thermal inertia of the equipment. Transformed fraction X was obtained from the integral of the heat flux (DSC signal) normalized to the area of the peak $\Delta H = 3302 \pm 24$ J mol⁻¹. It is worth noticing that as the peak shifts to higher temperatures, Ozawa's method is comparing the transformation in very different stages. Therefore, we limit our analysis to the range $0.1 < X < 0.9$, which corresponds to $-2.25 < \ln(-\ln(1 - X)) < 0.834$. This prevents the use of all the curves in a single analysis. Figure 7b shows the plot of $\ln(-\ln(1 - X))$ for temperatures between 432 and 438 K (1 K span) and Figure 7c shows the plot of $\ln(-\ln(1 - X))$ versus $\ln(\beta)$ in the range for which at least three β curves can be used.

The resulting Avrami exponent from Ozawa analysis is $n = 1.3 \pm 0.2$. Although the order of this value is correct, absence of nucleation or low-dimensional growth is hardly expected in the formation of the liquid.

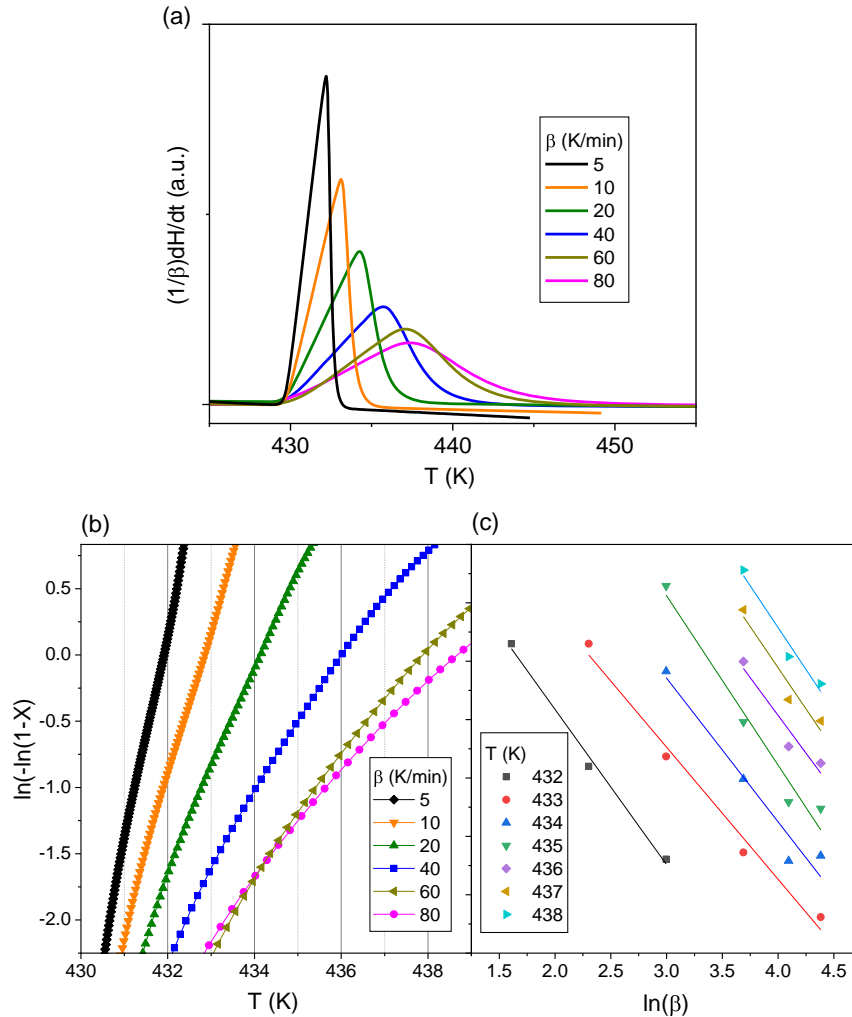


Figure 7. a) DSC signal of In standard sample in the melting region. b) $\ln(-\ln(1-X))$ as a function of temperature, and c) $\ln(-\ln(1-X))$ as a function of $\ln(\beta)$.

Returning to the Equation (23), it is worth mentioning that, for any transformation, the temperature range of interest is limited and when the transformation occurs in a sufficiently reduced temperature range, substituting the exponential for an effective average value leads to

$$X^*(T) = \frac{C}{\beta^{dn_G+1} n_G^d (dn_G + 1)} \exp\left(-\frac{Q_I + dQ_G}{k_B T}\right) (T - T_0)^{dn_G+1} \quad (24)$$

If we started from the second integral of Equation (3), we will recover something similar but dn_G would appear instead of $dn_G + 1$. Therefore, the direct application of KJMA-plot in the general nonisothermal case assuming an average temperature in the exponential leads to

$$\ln(X^*) = \left[-\frac{Q_I + dQ_G}{k_B T} - n \ln(\beta) + \ln(B) \right] + n \ln(T - T_0) \quad (25)$$

where B would be independent of temperature (although as it was pointed above for Ozawa's method, this implies that we have to neglect also any dependence of $B = \ln\left(\frac{C}{n_G^d (dn_G+1)}\right)$ on X or β). On the one hand, the simple relationship $n = n_G d + n_I$ can still be valid. Moreover, the intercept of KJMA-plot, $\ln(X_{int}^*) = \left[-\left\langle \frac{Q_I + dQ_G}{k_B T} \right\rangle - n \ln(\beta) + \ln(B) \right]$, depends on the heating rate and on the average temperature used to simplify the integrals.

This direct application of KJMA-plot to the melting of the indium standard sample was also performed in the present study. However, due to the high sensitivity of the results to the indetermination of the induction time (temperature in the case of nonisothermal regime) the procedure was done as follows: 1) KJMA-plots were generated using the estimated T_0 values from the measured T_{slope} using Equation (18). 2) The average slope of KJMA-plots in the range $0.1 < X < 0.9$ results $n = 4.3 \pm 0.6$, which is consistent with an interface controlled growth and constant nucleation rate. However, the plot of

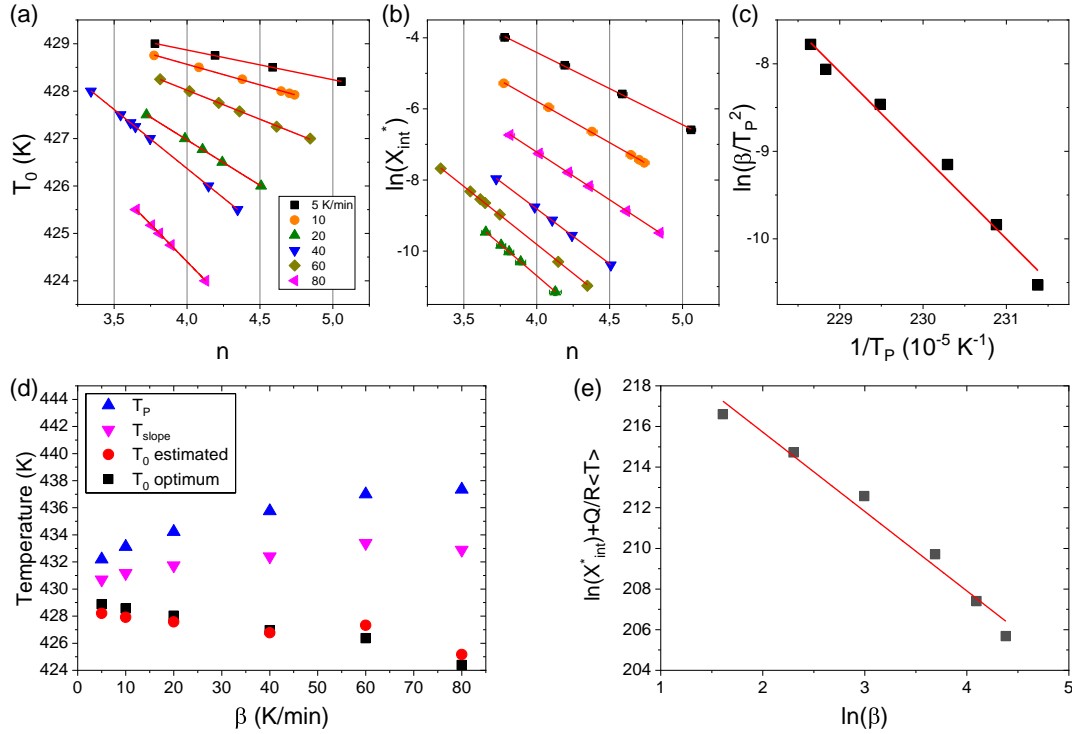


Figure 8. KJMA analysis applied to the melting of In standard. Relationship between Avrami exponent and a) the induction temperature, and b) $\ln(X_{int}^*)$. c) Kissinger plot to determine the activation energy Q . d) Peak temperature, T_P , and onset temperatures estimated from the steepest slope, T_{slope} , and from Equation (18), and optimum T_0 value chosen as the value leading to $n = 4$ in (a). e) $\ln(X_{int}^*) + \langle \frac{Q}{k_B T} \rangle$ versus $\ln(\beta)$ using the intercepts in (b) for the optimum T_0 and T_P as the average temperature.

$\ln(X_{int}^*) + \langle \frac{Q}{k_B T} \rangle$ ($Q = 790 \pm 50 \frac{\text{kJ}}{\text{mol}}$ from Kissinger's method^[69]) versus $\ln(\beta)$ with $\langle T \rangle \sim T_P$ (the peak temperature at which the transformation rate is maximum) yields an inconsistent $n \sim 2$, which is due to the strong effect of indetermination of T_0 . 3) Fine-tuning of the value of T_0 allows us to find the corresponding optimum T_0 values for $n = 4$ in KJMA-plots for each β . 4) Finally, using these values we obtain $n = 3.4$ ($n = 4.1$ neglecting low heating rates) as the slope of $\ln(X_{int}^*) + \langle \frac{Q}{k_B T} \rangle$ versus $\ln(\beta)$. **Figure 8a,b** show the dependence of T_0 and $\ln(X_{int}^*)$ with n ; **Figure 8c** shows the Kissinger plot to determine the activation energy Q ; **Figure 8d** shows the corresponding values of estimated T_0 , optimum T_0 , T_P , and T_{slope} for each β ; and **Figure 8e** shows the plot of $\ln(X_{int}^*) + \langle \frac{Q}{k_B T} \rangle$ versus $\ln(\beta)$.

Figure 9 shows the local Avrami exponents (a) and KJMA-plots (b) for the different heating rates in the range $0.1 < X < 0.9$.

In 1972, Nakamura et al.^[67] proposed an approximation for the Avrami equation to be extended to nonisothermal regimes, in which, $X^*(T)$, for constant heating rate, is expressed as

$$X^*(T) = \frac{1}{\beta^n} \left[\int_{T_0}^T k_0 \exp\left(-\frac{Q}{k_B T'}\right) dT' \right]^n \quad (26)$$

This approximation, developed for isokinetic transformations, is coherent with Ozawa's but comparing Equation (26) with (22)

shows that the former is an approximation compiling the temperature dependence in just one exponential Arrhenius-type dependence.

$$k_0^n \exp\left(-\frac{nQ}{k_B T}\right) \approx \int_{T_0}^T \frac{d}{dT'} \left\{ C \exp\left(-\frac{Q_i}{k_B \theta}\right) \left[\int_{\theta}^T (T' - T_R)^\alpha \exp\left(-\frac{Q_G}{k_B T'}\right) dT' \right]^d \right\} d\theta \quad (27)$$

However, Equation (26) is strictly equal to Equation (22) for transformations for which the growth is so fast that new crystals are only observed with its final size. These conditions define the instantaneous growth approximation ($d = 0$)^[70,71] and explains why a direct approach to nonisothermal conditions works so well in the case of nanocrystallization processes.^[72] This latter approximation, derived from Nakamura et al. work, assumes an effective onset temperature $T'_0 \sim T_P/2$, where T_P is the peak temperature (i.e., the temperature at which the transformation rate is maximum), to simplify Equation (26) to^[73]

$$X^*(T) = \frac{1}{\beta^n} \left[k'_0 \exp\left(-\frac{Q'}{k_B T}\right) (T - T'_0) \right]^n \quad (28)$$

The application of expression (19) to determine the local Avrami exponent is thus modified after taking into account the temperature dependence of the frequency factor

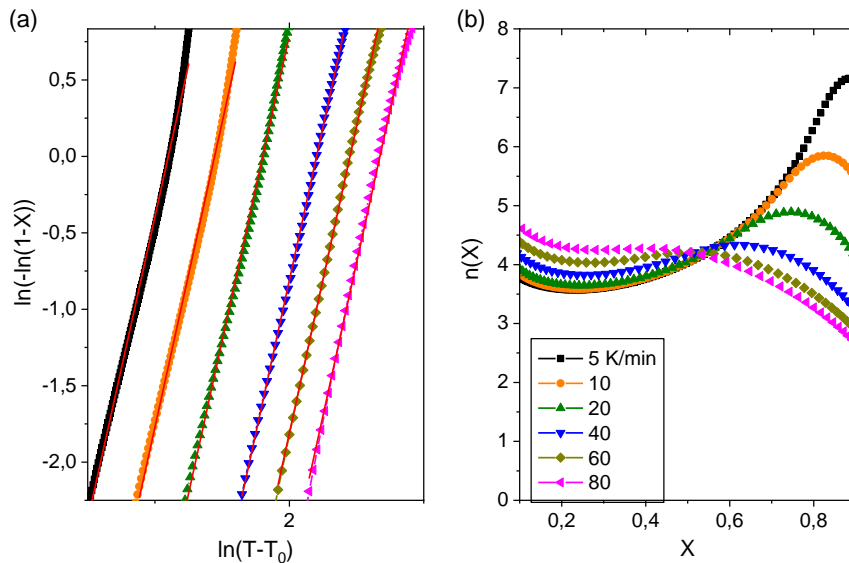


Figure 9. KJMA-plots a) and local Avrami exponent b) for melting process of an In standard sample at different heating rates.

$$n(X) = \frac{d \ln(-\ln(1-X))}{d \ln(t-t_0)} \left(1 + \frac{Q'}{k_B T} \left(1 - \frac{T'_0}{T} \right) \right)^{-1} \quad (29)$$

This approximation works well for very broad transformations (e.g., temperature range of nanocrystallization can be over 100 K) and presents the advantage over Ozawa's method that the local values $n(X)$ are obtained for a single non-isothermal experiment (which can be compared to experiments at other heating rates to study whether isokinetic behavior is observed). However, the average $n(T)$ from Ozawa needs to assume that at the same temperature (and very different X values for different β) the kinetic parameters are the same.

6. Effects of Breakdown of Kolmogorov Postulates

6.1. Deviation from the First Postulate of Kolmogorov: Overlapped Processes

A particular case of deviation from the first postulate occurs in overlapped processes. In this case, interpretation of application of KJMA theory is not straightforward. However, neglecting coalescence or other recrystallization processes, Avrami exponents of the individual processes can be extracted from the analysis of the effective Avrami exponent resulting from a direct KJMA analysis.^[74] To do this we can consider two different situations when two transformations overlap: 1) processes which are not competing for the same type of atoms and 2) processes which are competing for the same type of atoms. The former case implies that the geometrical impingement acts independently for each process and there are restricted regions for each transformation. The latter case implies that geometrical impingement is common to the different processes and evolution of one transformation restricts the progress of the other ones.

6.1.1. Independent Geometrical Impingement

This should occur when the processes are not competing for the same type of atoms and thus volume of the region to be transformed in product phase one is not overlapping with the volume of the region to be transformed in product phase two. This idea is summarized in the addition of the individual transformed fractions to obtain the total transformed one

$$X = \sum_i^N f_i X_i = \sum_i^N f_i (1 - \exp(-X_i^*)) \quad (30)$$

where f_i is the maximum transformed fraction corresponding to i process and $\sum_i^N f_i = 1$. Several consequences can be obtained from the study of the effective local Avrami exponent $n^*(X)$ (applying Equation (19) for isothermal case or Equation (29) for nonisothermal case) obtained in the limit case of nonoverlapped processes^[74]

Despite the individual processes were isokinetic, this behavior is not preserved in the effective Avrami exponent of the whole process, unless the different overlapped processes have the same activation energy.

When individual processes show different activation energies, their overlapping can be tuned by changing the annealing temperature (isothermal) or the heating rate (nonisothermal).

Transformed fractions of the different phases at the end of the process are independent of the annealing conditions or the heating rate.

The individual Avrami exponent of the earlier process, n_1 , can be recovered as the limit value $n_1 = \lim_{X \rightarrow 0} n^*(X)$.

The individual Avrami exponent of the last process, n_N , can be recovered from the behavior of $n^*(X)$ at high values of $X > 1 - f_N$

$$n_N = n^*(X) - \frac{dn^*(X)}{dX} (1 - X) \ln(1 - X) \quad (31)$$

Moreover, the fraction f_N corresponding to the last process can be also obtained from the analysis of $n^*(X)$ at high values of X

$$\ln(f_N) = -\frac{1}{n_N} (1 - X) [\ln(1 - X)]^2 \frac{dn^*(X)}{dX} \quad (32)$$

Equation (31) and (32) allow for deconvolution of two overlapped processes once recalculating $X_1 = X/(1 - f_2)$ and $X_2 = (X - (1 - f_2))/f_2$

This analysis has been applied to the crystallization of different amorphous Fe(Co)-Zr^[75,76] and Fe-Nb^[77] alloys. Moreover, the assumption of multiple overlapped microprocesses reproduces the low Avrami exponents found in nanocrystallization. Numerical calculations performed using numerous overlapped microprocesses with $n_i = 2.5$ successfully reproduced the experimental effective Avrami values found in the crystallization of FINEMET alloys.^[78]

6.1.2. Common Geometrical Impingement

When geometrical impingement affects to all the overlapped processes in a common way, the total extended transformed fraction can be calculated as the addition of the different individual contributions^[74,79] leading to

$$X = 1 - \exp\left(-\sum_i^N X_i^*\right) \quad (33)$$

And the individual rates of transformations can be expressed as

$$\frac{dX_i}{dt} = (1 - X)^\eta \frac{dX_i^*}{dt} \quad (34)$$

In the case of two overlapped processes fulfilling this condition with $\eta = 1$, several statements can be derived^[74]:

- 1) The overlapped process cannot be experimentally deconvoluted: when one of the processes is delayed, its fraction becomes reduced.
- 2) Transformed fractions at the end of the complete process depend on the annealing conditions or the heating rate.
- 3) As it occurs in noncompetitive processes, isokinetic character is not preserved for the effective Avrami exponent. In the case of competitive processes, nonisothermal analysis using Equation (29) showed that, for a given transformed fraction X , $n^*(X)$ increases with the heating rate if the activation process is higher for the process with the highest Avrami exponent. On the other hand, $n^*(X)$ decreases with β when the activation energy is higher for the process with the lowest Avrami exponent.

This analysis was applied to the nanocrystallization of α -Fe(Ga) of bulk amorphous alloys with the presence of quenched in crystallites of this phase.^[73]

6.2. Deviation from the Fourth and Fifth Postulates of Kolmogorov

6.2.1. Overgrowth in Diffusion Controlled Growth Processes

As it was shown in Figure 2a, for those transformations in which the growth rate is decelerated, when statistically a phantom nucleus appear close to the edge of an already growing crystal, its faster growth rate may lead to an overgrowth region accounted by KJMA expression. In order to appreciate the importance of this effect in diffusion controlled growth, we have performed simple simulations in 1D space using MatLab. The simulation acts iteratively, being each iteration step a time unit. We define a line of length L (with boundary conditions) and each iteration step a nucleus is formed in a random point of the line. The radius of a nucleus formed at iteration step τ is updated every iteration step t as: $r(t, \tau) = A\sqrt{(t - \tau)}$ following Equation (12) (parameter A was tailored between $A/L = 2 \times 10^{-5}$ to $2 \times 10^{-3} \text{step}^{-0.5}$), which allows us to obtain the extended transformed fraction, X^* , adding the size of each formed region (phantom and real ones) divided by L . Once a new nucleus is formed we labeled whether the nucleus is real or phantom (the nucleation point belongs to an already transformed region). To obtain the actual transformed fraction we check equidistant points in the line and distinguish whether the point belongs to an already transformed region or not and, in the former case, whether the transformed region is covered only by a phantom crystal. This procedure allows us to obtain the actual transformed fraction, X , as well as the overgrowth fraction, X^{over} . The latter is the transformed fraction only covered by the growth of a phantom nucleus.

Figure 10 summarizes the results obtained from the simulations for an average over 100 curves with $A/L = 2 \times 10^{-4} \text{step}^{-0.5}$. Figure 10a,b show X and X^{over} , respectively, as a function of the iteration step. As expected, X^{over} is null at the beginning (negligible probability to appear a phantom nuclei) and at the final stages (negligible probability of a phantom nuclei to appear close to an active boundary). Moreover, the maximum X^{over} is about 1.5%. Symbols in Figure 10c show the relation between X and $1 - \exp(-X^*)$. Regression is fairly good ($R^2 = 0.99997$) with a slope of 0.9921 ± 0.0002 . Linear fitting of $X + X^{\text{over}}$ versus $1 - \exp(-X^*)$ leads to $R^2 = 0.99999$ and slope of 1.00024 ± 0.00008 , showing the expected improvement in correlation. Finally, Figure 10d shows the KJMA-plot from which Avrami exponent is obtained for $0.05 < X < 0.95$ as $n = 1.4807 \pm 0.0006$. The difference with respect to the theoretical Avrami value for constant nucleation rate and diffusion controlled growth, $n = 1.5$ (see Table 1) is below the typical errors obtained in the experiments and therefore, KJMA theory seems to be a fairly good approximation to describe the diffusion controlled growth processes. Changes in parameter A lead to the same conclusions.

6.2.2. Mechanical Amorphization of Ball Milled Powders

KJMA theory assumes that a nucleus is formed in a very small region, which can be even approximated to a point as we did in Equation (7). From this point-like nucleus, the spherical transformed region grows. We pointed the possibility of anisotropic

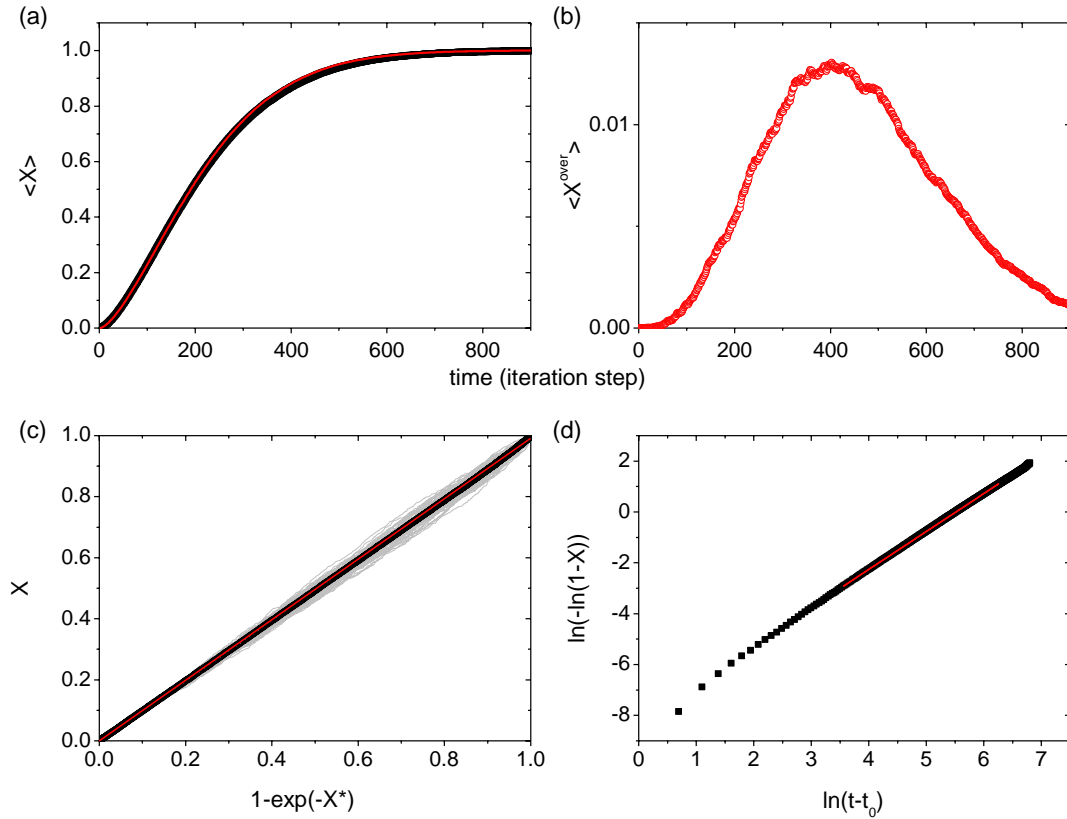


Figure 10. Results from 1D simulation of diffusion controlled growth with $A/L = 2 \cdot 10^{-4} \text{ step}^{-0.5}$. a) Averaged actual transformed fraction, $\langle X \rangle$ over 100 curves (black symbols) and plus averaged overgrowth fraction (red line) as a function of simulated time (iteration step); b) average overgrowth fraction as a function of time; c) actual transformed fraction as a function of the theoretically predicted one by KJMA model from the extended transformed fraction, red line corresponds to the linear fitting fixing the intercept to zero (individual curves appear as grey lines); and d) KJMA-plot (symbols) and fitted straight line (red line) resulting in $n = 1.4807 \pm 0.0006$.

growth in Equation (6A), which describes an ellipsoidal shape for the growing transformed region. Any of these cases fulfill the convex shape required by the fourth postulate. However, mechanical amorphization,^[80,81] first reported by Yermakov et al.^[82] and Koch et al.^[83] in early 1980, is a solid-state transformation which disobeys the fourth postulate. This transformation practically occurs at a constant temperature as stationary condition (about 10 K rise in vial temperature) is rapidly achieved in planetary mills.^[84] In mechanical amorphization, concerning first postulate, the amorphous phase can completely substitute the supersaturated solid solution previously formed during milling. Concerning the second postulate, the size of the regions to be amorphized is in the order of 5–10 nm and the third postulate is fulfilled from a global point of view. Moreover, concerning the fifth postulate, a constant linear growth rate of the amorphous regions (interface controlled) is feasible as the amorphous-crystalline boundary advances at low temperature in a supersaturated solid solution where, once it is formed, diffusion should not be the determinant mechanism.

During mechanical amorphization, the polycrystalline powder particles become mixed and, independently whether the powder becomes comminuted or agglomerated, the size of the crystallites progressively reduces to nanoscale.^[80,81,84] From this nanocrystalline supersaturated solution, some compositions amorphize. This

solid-state transformation does not fulfill the fourth postulate of Kolmogorov as the transformed regions are concave (the nanocrystals become progressively amorphous from the surface to the core). This fact completely changes the functional form of the extended transformed volume, which should be^[85]

$$X^* = \frac{D_0^3 - (D_0 - 2L(t))^3}{D_0^3} = 1 - \left(1 - 2\left(\frac{L_0}{D_0} + \frac{u}{D_0}(t - t_0)\right)\right)^3 \quad (35)$$

where D_0 is the initial diameter of the nanocrystals; $L(t) = L_0 + u \cdot (t - t_0)$ is the thickness of the amorphous layer, with L_0 its initial value; u , the linear growth rate and t_0 the induction time. Equation (29) can be rewritten as a third-order polynomial shifted in time to $(t - \tau_0)$

$$-\ln(1 - X) = X^* = A \cdot (t - \tau_0) + B \cdot (t - \tau_0)^2 + C(t - \tau_0)^3 \quad (36)$$

with $\tau_0 = t_0 - L_0/u$; $A = 6u/D_0$; $B = -12(u/D_0)^2$, and $C = 8(u/D_0)^3$. It is worth mentioning that, whereas in KJMA model we have three parameters to fit the transformation curve (k , t_0 , and n , as shown in Equation (1)), in Equation (34) there are only two fitting parameters: τ_0 and (u/D_0) . However, we

can flexibilize the requirements by using independent A , B , and C parameters in Equation (36) and to check how the relation between them departs from the theoretical one. This model was successfully applied to the amorphization of mechanically alloyed Fe–Nb–B alloys.^[85]

This analysis is here applied to the mechanical amorphization of two binary alloys: Fe₇₀Zr₃₀ and Fe₇₀Nb₃₀ produced by mechanical alloying.^[86] The amorphous fraction X was measured from Mössbauer spectrometry, which is a very sensitive technique to detect tiny fractions of paramagnetic (ferromagnetic) Fe sites contributions in ferromagnetic (paramagnetic) matrices. However, in the case of mechanical alloying, the earlier paramagnetic Fe sites must correspond to those Fe atoms in still remaining Nb of Zr crystals^[86] but not in amorphous phase. This may affect the determination of the induction time. **Figure 11** shows $X^* = -\ln(1 - X)$ as a function of the milling time for Fe₇₀Zr₃₀ and Fe₇₀Nb₃₀ mechanical alloys and fitted to Equation (36). **Table 2** collects the resulting data. Assuming an induction time $t_0 \approx 5$ h, the starting layer of amorphous phase is $L_0 < 1$ nm.

In a series of papers, Delogu et al.^[87–89] developed a different kinetic model to describe mechanically induced transformation during milling. This model is based on the probability of an untransformed region to be trapped a certain number of collisions that will deterministically drive the transformation of that region. The transformed fraction (extended transformed fraction is not considered in this model) is

$$X = 1 - e^{-fj} \left(1 + \sum_{i=2}^j \frac{(fj)^{i-1}}{(i-1)!} \right) \quad (37)$$

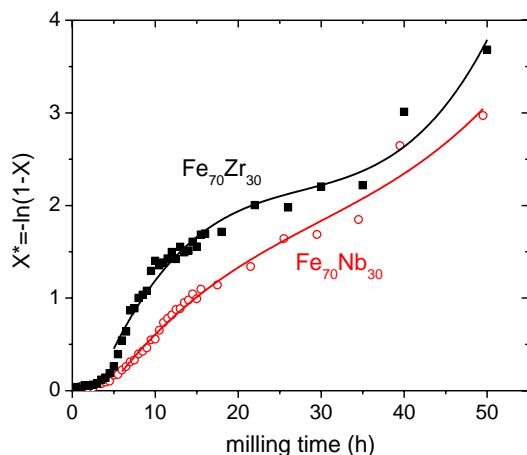


Figure 11. Extended transformed fraction as a function of the milling time for mechanical amorphization of Fe₇₀Nb₃₀ and Fe₇₀Zr₃₀ alloys along with the corresponding fittings to Equation (36).

Table 2. Parameters obtained from fitting evolution of amorphous fraction to Equation (36).

	τ [h]	$\frac{D_0}{u}$ [h ⁻¹]	D_0 [nm] ^[86]	u [nm h ⁻¹]
Fe ₇₀ Zr ₃₀	2.7 ± 0.4	0.028 ± 0.003	10 ± 2	0.28 ± 0.09
Fe ₇₀ Nb ₃₀	4.2 ± 0.5	0.0174 ± 0.0011	5 ± 2	0.09 ± 0.04

where f is the fraction of sample trapped in a collision, and q the total number of collisions at time t . This equation is further simplified by Delogu and Cocco^[87] assuming that transformation occurs after a single event and, changing from discrete parameter number of collisions q to continuous parameter time t , then

$$X = 1 - \exp(-k_{\text{col}}t) \quad (38)$$

And now k_{col} is the fraction of sample trapped in collisions per unit time. This kinetic expression is equivalent to KJMA with $n^* = 1$, which also agrees with the results of direct application of KJMA analysis to mechanical amorphization, with $0.5 \leq n^* \leq 1.5$.^[90–97]

The ideas of concave growth of amorphous layers to degrade the nanocrystals as well as the probabilistic character of the nucleation phenomenon (P is the probability of activation of a fraction f trapped in the collision to drive the amorphization) were implemented with the statistical model of Delogu.^[98] This was done in order to improve the description at short milling times assuming a distribution of induction times instead of a single value used in the study by Blázquez et al.^[85] However, the model (in the following, the extended concave model) does not yield simple expressions but numerical solutions are needed. Comparison of the extended concave model and Delogu's one assuming more than one event to drive amorphization leads to the following conclusions:

1) Development of Delogu's model predicts a maximum in the transformation rate depending on the number of collisions needed to drive the transformation j and frequency parameter k at time

$$t_{\text{max}} = \frac{j-1}{k_{\text{col}}} \quad (39)$$

2) This time for maximum transformation rate, which is observed in experiments at $t_{\text{max}} \neq 0$,^[98] is not predicted neither by KJMA model with $n^* = 1$ nor by Delogu's model with $j = 1$.

3) When results from Delogu's model are fitted to an effective KJMA curve, the effective Avrami exponent, n^* , increases from 1 to ≈ 2.4 as the number of collisions required for transformation increases, whereas the effective frequency factor, k_{eff} decreases with j .

4) KJMA analysis applied to the extended concave model predicts $n^* = 1$ for $\frac{PL_0}{u} \ll 1$; $n^* = 1.15$ for $\frac{PL_0}{u} \gg 1$ and a peak of $n^* = 1.5$ at $\frac{PL_0}{u} \approx 5$. These predictions are in a better agreement with the reported Avrami exponents^[90–97] than those from Delogu's model.

5) In the case of k_{eff} from KJMA analysis, for $\frac{PL_0}{u} \ll 1$, $k_{\text{eff}} = Pf$, i.e., growth rate is so fast that information on growth processes is lost and the frequency factor only informs about the nucleation frequency.

6) For $\frac{PL_0}{u} \gg 1$, corresponding to high nucleation probability or slow growth rate, k_{eff} decreases being $k_{\text{eff}} \approx 3fu/L_0$ allowing us, theoretically, to obtain information on the linear growth rate.

7) The extended concave model predicts a steady state between activation of new regions and the growth of the amorphous phase. In this steady state, a saturation value of the size of the

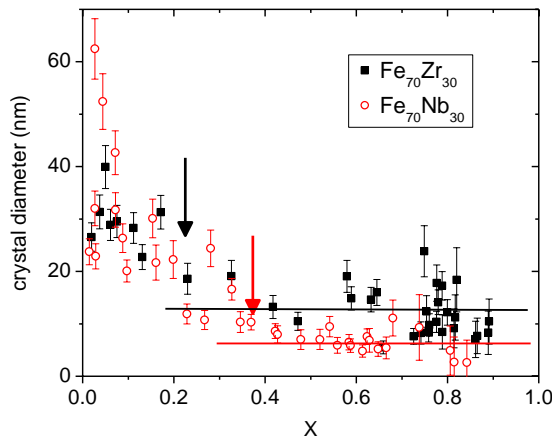


Figure 12. Size of the remnant crystallites as a function of the amorphous fraction for mechanical amorphization of $\text{Fe}_{70}\text{Nb}_{30}$ and $\text{Fe}_{70}\text{Zr}_{30}$ alloys. The arrows approximately indicate the corresponding transformed fraction, $X_{\text{Am}}^{\text{sat}}$, at which a constant size of the remnant crystallites, R_{sat} , is achieved. The horizontal lines indicate the corresponding R_{sat} values.

remnant crystallites, R_{sat} , appears at amorphous fractions above a certain value, $X_{\text{Am}}^{\text{sat}}$.

8) Moreover, the extended concave model predicts these two magnitudes rescale with $\frac{PL_0}{u}$. For $0.01 < \frac{PL_0}{u} < 10$, relative values of R_{sat} decreases from 1 to 0 and $X_{\text{Am}}^{\text{sat}}$ increases from 0 to 1. In fact, for $u \gg$, the transformed regions almost amorphize instantaneously and remnant crystallites are only those which are not still activated. For $u \ll$, there is no saturation in the size of the remnant crystallites.

The point (8) can be the reason why we observed a larger size of the remnant crystallites in $\text{Fe}_{70}\text{Zr}_{30}$ than in $\text{Fe}_{70}\text{Nb}_{30}$ alloy^[86] (see Table 2). As it is shown in **Figure 12**, crystal size is smaller for $\text{Fe}_{70}\text{Nb}_{30}$ alloy and the saturation value is achieved at a higher $X_{\text{Am}}^{\text{sat}}$ than for $\text{Fe}_{70}\text{Zr}_{30}$ alloy. In fact, a reduction of 50% in R_{sat} corresponds to about threefold increase in $\frac{PL_0}{u}$ parameter,^[98] which is in agreement with the observed change in the growth rate u in Table 2.

The extended concave model, considering the probability of activation of regions after a fixed number of collisions, could be also extended to other mechanically driven physical transformations observed during milling, such as mechanically induced nanocrystallization for which values of $n^* \approx 1.5$ are reported.^[99,100]

6.3. Instantaneous Growth Approximation

The way the transformation of a certain process is registered (the characteristic acquisition time) affects the information available from the time evolution of the transformed fraction. This is the case when growth is strongly impinged, as in nanocrystallization processes.^[70,71,101,102] On the other hand, very fast growth, as it occurs in martensitic transformations (in the order of the speed of sound^[36]), prevents from registering the time a crystal is growing by using conventional calorimetric or similar methods to follow the transformation. Therefore, once a nucleus is formed, the contribution to the measured property

(e.g., enthalpy, magnetization, resistivity, etc.) corresponds to the crystal with its final size.

6.3.1. Effective Values of Avrami Exponent in Instantaneous Growth Processes

In the instantaneous growth model, the only information available corresponds to nucleation phenomenon and for isothermal conditions, Equation (3) can be simplified to

$$X^*(t) = V_c \int_0^t I(\tau) d\tau = V_c \int_0^t I_0 \exp\left(-\frac{Q_I}{k_B T}\right) d\tau \quad (40)$$

where V_c is the volume of the crystals and Arrhenius dependence has been assumed for nucleation rate, whereas for nonisothermal conditions Equation (21) can be simplified to

$$X^*(T) = \frac{V_c}{\beta} \int_{T_0}^T I_0 \exp\left(-\frac{Q_I}{k_B \theta}\right) d\theta \quad (41)$$

As it was commented above, this expression is a particular case of Nakamura's equation (for $n = 1$). Taking into account Equation (40) and (41) and (15), we can obtain the nucleation rate for isothermal regimes

$$I(X(t)) = \frac{1}{V_c} \frac{dX^*}{dt} = \frac{1}{V_c(1-X)^n} \frac{dX}{dt} \quad (42)$$

And for nonisothermal regimes

$$I(X, T) = \frac{\beta}{V_c} \frac{dX^*}{dT} = \frac{\beta}{V_c} \frac{1}{(1-X)^n} \frac{dX}{dT} \quad (43)$$

In order to understand how this interpretation departs from KJMA analysis, **Figure 13** shows application of Equation (42) to theoretical KJMA curves for different values of the Avrami exponent ($n > 1$, indicating increasing nucleation rate). For $n = 1$, both interpretations are fully coherent and in this case the classical Koistinen–Marburger^[103] equation to determine the amount of remnant austenite in quenching experiments can be justified.^[104,105] For $n > 1$, an apparent increase in the nucleation rate would be appreciated or vice versa (i.e., transformation for which nucleation increases would show effective Avrami exponent above 1). Fitting curves of Figure 13 to straight lines in the $0.1 < X < 0.9$ range leads to a relative value of the intercept at $X = 0$, $I(0)/I(0.5)$, which decreases from 1 to almost zero as n increases from 1 to 4. Moreover, the departure from linearity of this apparent increase in $I(X)$ increases as n increases. This preliminary discussion would be helpful in discussing the adequacy of instantaneous growth approximation to the two cases that will be shown below.

6.3.2. Simulations Performed in the Frame of Instantaneous Growth

In order to explore how instantaneous growth processes depart from KJMA predictions, we have performed simulations based

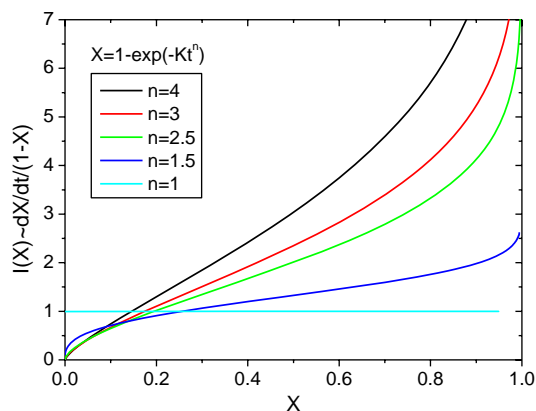


Figure 13. Application of instantaneous growth analysis to theoretical KJMA curves for different values of the Avrami exponent. An increasing nucleation rate with the transformation is reproduced for effective Avrami exponent above 1.

on 2D cellular automata. We explore the transformation of a square formed by 1000×1000 cells using two parameters, a constant nucleation rate, I (number of nuclei formed per step), and a maximum linear size of the nuclei, $2D - 1$ cells. In every simulation step, a number of nucleation sites are randomly chosen. For those sites corresponding to untransformed cells, the nuclei grow to their maximum size, taking into account the geometrical impingement between the contemporary and earlier nuclei. At every iteration step, the transformed fraction is obtained.

Figure 14 shows the simulated microstructure formed. For low enough values of $I \cdot D^2$ regularly shaped crystallites can be identified, whereas irregular crystals due to geometrical impingement appear as $I \cdot D^2$ increases.

Results of the effective KJMA analysis on the simulated results are summarized in **Figure 15**. This figure shows that KJMA-plot can be generally described as a two slope curve. Effective Avrami

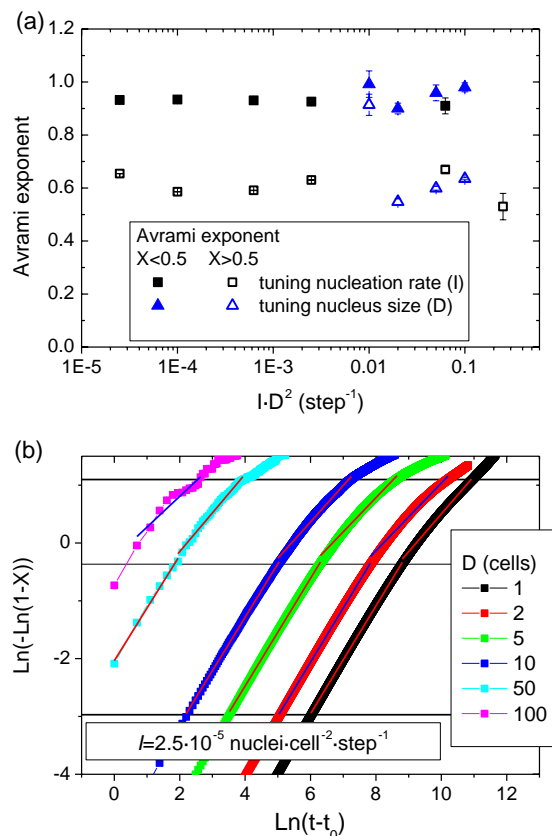


Figure 15. a) Avrami exponents obtained from KJMA-plots fitted to straight lines in the ranges $0.05 < X < 0.5$ (solid symbols) and $0.5 < X < 0.95$ (hollow symbols) as a function of the product of the nucleation rate and the square of the crystal size (number of cells allowed for linear growth). Triangles correspond to results from tuning the crystals size, D , for nucleation rate $I = 250$ nuclei/steps (upper row in Figure 14). Squares correspond to results from tuning I for $D = 100$ cells (lower row in Figure 14). b) KJMA-plots corresponding to the microstructure developed in the upper row of Figure 14.

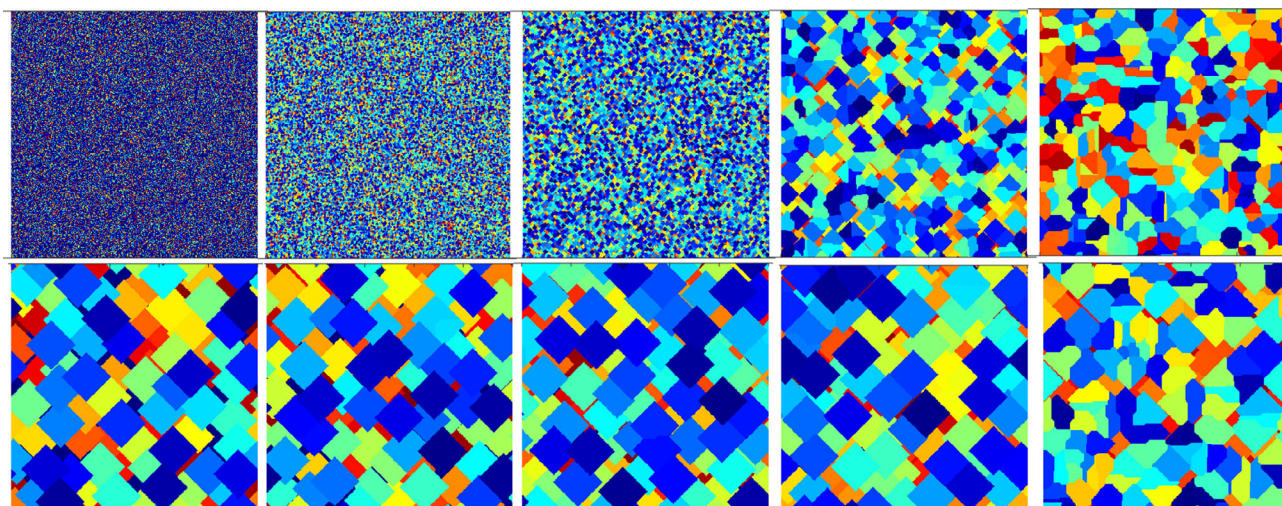


Figure 14. Simulated 2D microstructures in the frame of instantaneous growth processes. Upper row corresponds to a nucleation rate of 250 nuclei/steps in a 10^6 cells space which linearly grows 1, 2, 5, 10, 50, and 100 cells (from left to right) before a new nucleation event occur. Lower row corresponds to nucleation rates of 1, 2, 5, 10, and 100 nuclei/steps (from left to right) which linearly grows 100 cells.

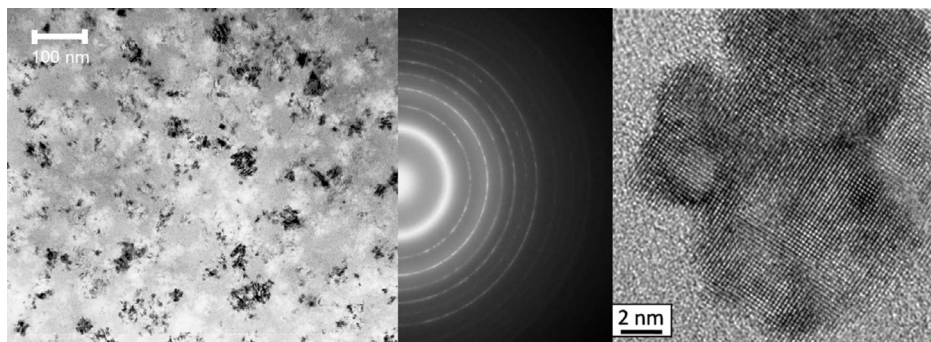


Figure 16. Bright field image (left), selected area diffraction pattern (center), and high resolution transmission electron image (right) of a nanocrystallized $\text{Fe}_{60}\text{Co}_{18}\text{Nb}_6\text{B}_{16}$ alloy (further details in ref. [71]).

exponents obtained from linear regression of KJMA-plot in the range $0.05 < X < 0.5$ lead to $n \approx 0.93$, which is close to the theoretical prediction of KJMA for a constant nucleation process without growth ($n = 1$). However, deviations appear at high transformed fractions and $n \approx 0.6$ is found in the range $0.5 < X < 0.95$.

6.3.3. Instantaneous Growth Process Applied to Nanocrystallization

The instantaneous growth model was applied to nanocrystallization processes.^[70,71] Equation (42) and (43) were applied to

the nanocrystallization of melt-spun amorphous ribbons of $\text{Fe}_{60}\text{Co}_{18}\text{Nb}_6\text{B}_{16}$ composition using $\eta = 1$. This alloy shows, after nanocrystallization, a microstructure formed by spherical nanocrystals of ≈ 5 nm diameter but agglomerated in groups of ≈ 20 nm embedded in a residual amorphous matrix (Figure 16).

Figure 17a,b shows, for as-melted ribbons, the isothermal and nonisothermal DSC scans recorded in a Perkin-Elmer DSC7 calorimeter calibrated using the melting temperatures of lead and K_2CrO_4 standards, and Figure 17c shows the local Avrami exponents obtained using Equation (19) and (29), respectively. Average value of $n \approx 0.25$ from Ozawa's method is also shown. Combining isothermal and nonisothermal experiments is highly recommended to determine kinetic properties as concluded

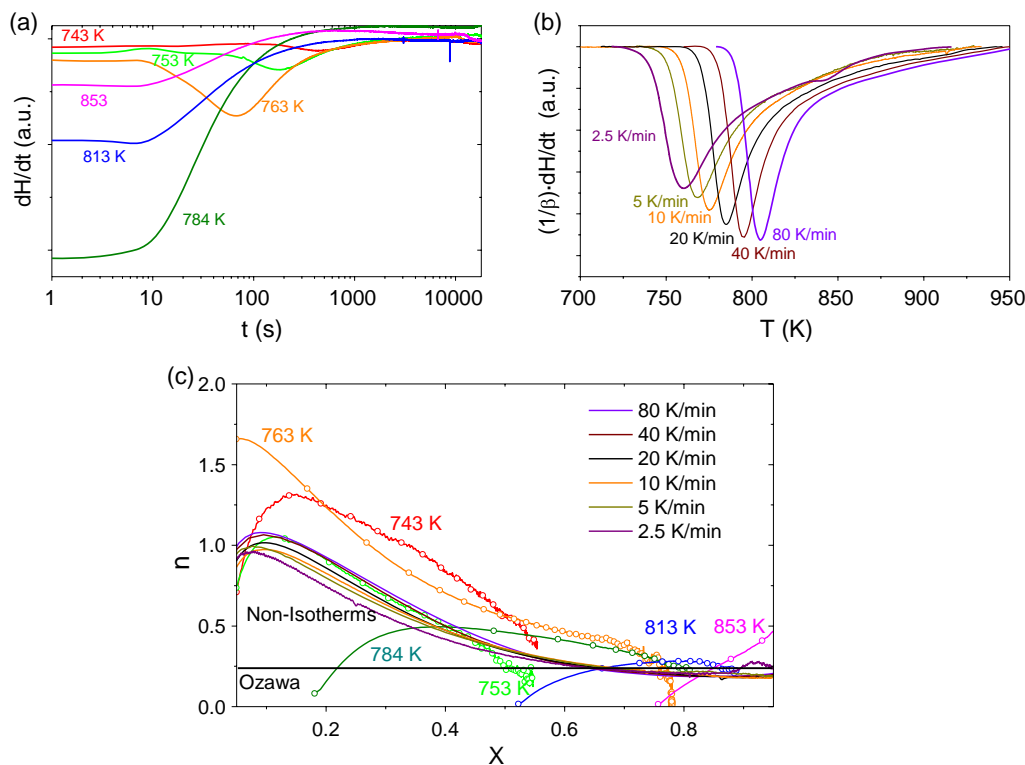


Figure 17. a) Isothermal DSC scans, b) nonisothermal DSC scans, and c) local Avrami exponent from Equation (19) and (29) for the nanocrystallization process of $\text{Fe}_{60}\text{Co}_{18}\text{Nb}_6\text{B}_{16}$ alloy. The horizontal line in (c) corresponds to the value of n obtained from Ozawa's method.

by the International Confederation for Thermal Analysis and Calorimetry (ICTAC).^[37]

Figure 18a shows the nucleation rate I as a function of transformed fraction X and, finally, Figure 18b shows the value of $I_0(X)$ assuming an Arrhenius dependence for $I(X, T)$. Kissinger method was used to obtain the activation energy $Q = 380 \pm 20 \text{ kJ mol}^{-1}$ ($Q = 3.9 \pm 0.2 \text{ eV at}^{-1}$).^[106]

From KJMA analysis, isokinetic behavior can be observed and low n values should be interpreted qualitatively as characteristic of a strongly impinged process. In the frame of the instantaneous growth approximation, it can be observed that isothermal nucleation rate is not constant along the process but it initially increases and then decreases. This behavior is coherent with the values of $n(X)$, which initially increases above 1 and then decreases below 1. The early increase in $I(X)$ ($n(X) > 1$) is ascribed to a second nucleation mechanism in the surface of already formed nanocrystals (leading to the formation of agglomerates). After the maximum, the continuous decrease in $I(X)$ ($n(X) < 1$) was understood due to the depletion of the amorphous matrix in Fe. Although this semiquantitative analysis agrees with the isothermal values of $I(X)$, it does not correspond to the $I(X)$ values obtained in nonisothermal conditions (see an almost constant value in Figure 18a). This is due to the strong effect of the exponential dependence on temperature, which enhances nucleation rate. Moreover, the decrease in the

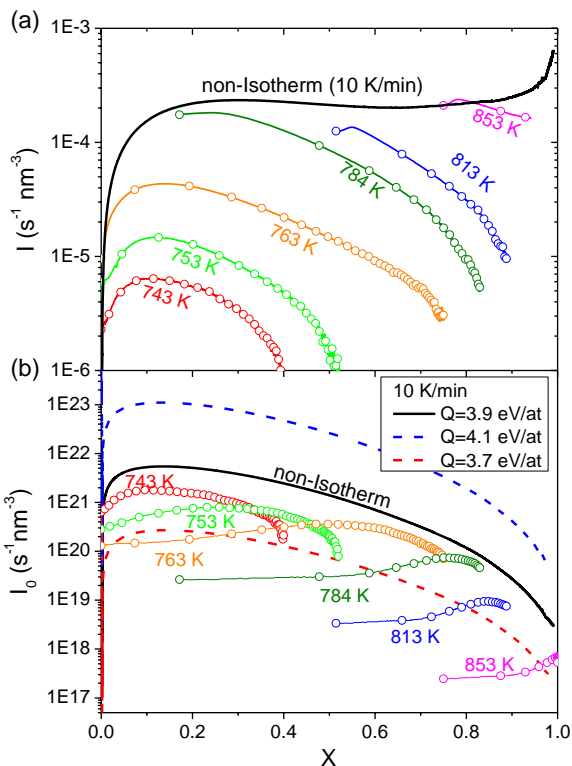


Figure 18. a) Nucleation rate from isothermal and non-isothermal (at 10 K min^{-1}) DSC scans as a function of the transformed fraction and b) prefactor of the nucleation rate to compare the curves independently of the temperature. Dashed lines corresponds to the nonisothermal scans calculated using the extreme values of the activation energy taking into account its error bar ($\pm 0.2 \text{ eV at}^{-1}$).^[106]

Avrami exponent as the transformation progresses agrees with the previous simulations shown here.

It is worth reminding that the assignment of decreasing nucleation rate as $n_l < 1$ (or increasing I as $n_l > 1$) is based on a functional form of the nucleation rate $I(t) = t^a$. If this is not the case, and nucleation rate changes during the transformation, the relationship between Avrami exponent and evolution of $I(t)$ is no longer straightforward. However, in Figure 18b a fairly good agreement is observed for $I_0(X)$ for isothermal and non-isothermal curves. This is found despite the simple Arrhenius approximation used and the strong effect of Q (see dashed lines in Figure 18b).

6.3.4. Instantaneous Growth Process Applied to Martensitic Transformation

As an example of martensitic transition, we present the martensite to austenite transformation of a $\text{Ni}_{50.53}\text{Mn}_{33.65}\text{In}_{15.82}$ metamagnetic shape memory alloy. This system has a change at $\approx 285 \text{ K}$ from paramagnetic martensite to ferromagnetic austenite on heating. Therefore, the transformation can be registered from the change in specific magnetization $\sigma(H, T)$ (see upper inset in Figure 19) as well as from calorimetric measurements.^[107]

Isothermal curves as a function of the applied magnetic field, $\mu_0 H$, were obtained in a Lakeshore 7407 vibrating sample magnetometer (VSM) with LN2 cryostat.^[107] Specific heat, c_p , measurements were obtained at a very slow rate ($\beta \approx 0.1 \text{ K h}^{-1}$)^[107] in a home-made calorimeter^[108] following a protocol that prevents the measurement of latent heat ascribed to the transformation.^[109]

Figure 19 shows $X(\mu_0 H)$ curves from the isothermal curve obtained at 285 K. In order to extract $X(\mu_0 H)$, the specific

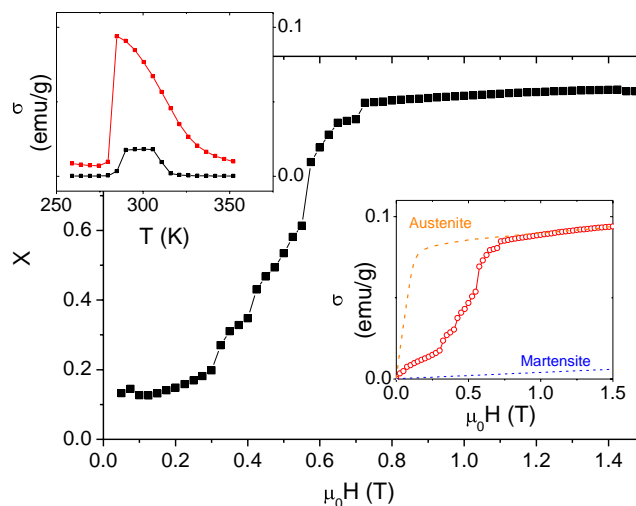


Figure 19. Main panel: austenite fraction from specific magnetization as a function of magnetic field at 285 K for a Ni–Mn–In alloy. Upper inset: temperature dependence of specific magnetization at 25 mT (black) and 1.5 T (red). Lower inset: isothermal magnetization curve at 285 K (red symbols) along with the estimated magnetization curves of the pure martensite (blue dashed line) and the austenite (orange dashed line) phases.

magnetization of both pure martensite and pure austenite phases was estimated at 285 K. In the case of pure martensite phase, a linear field dependence is assumed which slope was extrapolated from the values of the slopes of the magnetization curves in the range $265 \leq T \leq 275$ K. In the case of pure austenite phase, the magnetization curve measured at 290 K was rescaled to the saturation value of the isothermal curve at 285 K. The corresponding estimated values of specific magnetization along with the experimental isothermal curve at 285 K are shown in the lower inset of Figure 19.

On the other hand, the ferromagnetic behavior of austenite phase leads to an extra contribution to the specific heat with respect to the paramagnetic martensite (see inset of **Figure 20**). Therefore, an abrupt change in c_p is observed in the transition. Above 310 K, c_p falls due to the Curie transition of the austenite phase. This allows us to understand the change of c_p during the transition as a sum rule of the weighted contribution of each phase: $c_p = (1 - X)c_p^M + Xc_p^A$ (superindex M and A identify the martensite and austenite phases, respectively). Therefore, $X(T)$ can be obtained and it is shown in Figure 20.

Despite the controversy^[110,111] about the athermal (nonthermally activated) or isothermal (thermally activated) character of martensitic transformations, an effective KJMA analysis can be performed. However, the meaning of the resulting parameters may be out of the frame of the KJMA theory. In fact, several kinetic models developed for martensitic transformations yield equivalent expressions for the transformed fraction to KJMA with effective Avrami exponents $n^* = 1$ ^[103] and $n^* = 2$ ^[104]

The corresponding KJMA-plots for isothermal and nonisothermal curves are shown in **Figure 21** for the $0.1 < X < 0.9$ range. The effective Avrami exponents are $n^* \approx 3.5$ for isothermal magnetization curve and $n^* \approx 5$ for nonisothermal specific heat curve. In both cases, the onset values were estimated to be $H_0 = 0$ T and $T_0 = 279.5$ K, respectively, using analogous equations to Equation (18) and assuming $n = 4$. It has been discussed above how indetermination in the onset affects, particularly at high values of n . Moreover, we have neglected any field and/or temperature dependence of the kinetic parameters, using an average exponential as it was done in the case of the melting of indium. For athermal processes, this would not be a limitation but it should be important in the case of thermally activated

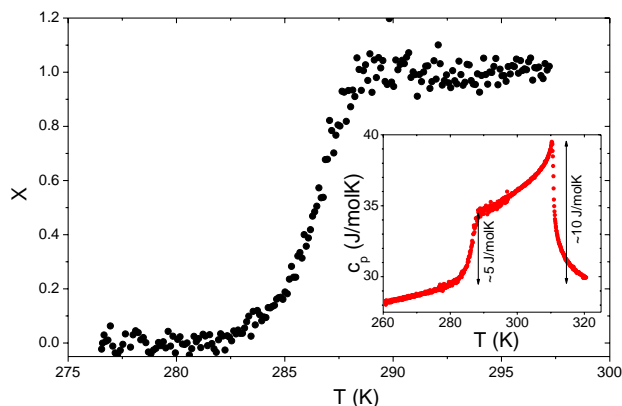


Figure 20. Austenite fraction estimated from specific heat measurements. Inset: specific heat as a function of temperature.

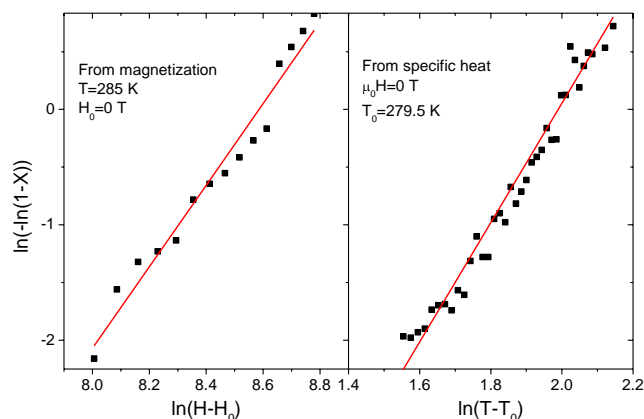


Figure 21. KJMA-plots for austenite formation from isothermal magnetization curves at 285 K (left) and from specific heat measurements (right).

processes. In the frame of KJMA theory, a 3D interface controlled growth with constant nucleation will be roughly in agreement with the resulting values of n .

However, taking into account the high speed of growth in martensitic transformations, in the frame of an instantaneous growth, these results should just mean that nucleation rate is increasing during the process as it is shown in **Figure 22**. This figure shows the transformation rate (although with respect to field change and temperature change, respectively) divided by the untransformed fraction, i.e., a magnitude proportional to $I(X)$ once field change and heating rate are constant,

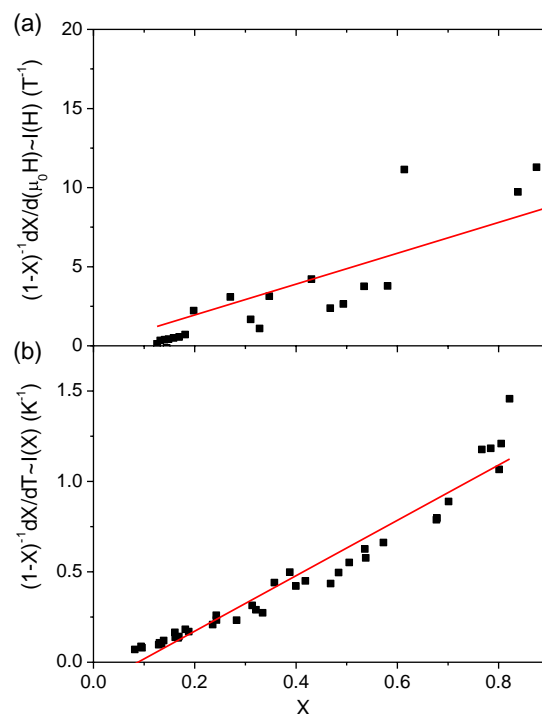


Figure 22. Nucleation rate (arbitrary units) as a function of the transformed fraction a) from isothermal magnetization curves at 285 K and b) from specific heat measurements.

respectively. This increase, approximately linear, should indicate that new nucleation sites appear in contact with the already transformed regions.

This leads to an expression of the transformation rate: $\frac{dX}{dt} = k_M X(1 - X)$, which corresponds to the kinetic equation of an autocatalytic transformation of the first order^[35] which has been used to describe the kinetics of martensitic transformation of Ni–Fe–Ga alloys.^[105]

In the case of the martensite-to-austenite transformation studied here, a KJMA process with $n = 4$ and a first-order autocatalytic transformation yields similar and apparently satisfactory descriptions of the transformation curve. However, the interpretation of the data yields strongly different mechanisms depending on the model assumed. In the former case, although an interface controlled growth is feasible in martensitic transformation, $n = 4$ also implies a constant nucleation rate without no activation of new nucleation sites and a 3D growth despite the lath structure of martensitic samples. Moreover, the problem arises when we consider the growth rate of martensitic transformations, which is in the order of hundreds of meters per second. This high speed implies that our acquisition time (≈ 20 and 720 s in the magnetic and specific heat measurements) is much larger than the time an austenite region grows to its final size. Therefore, the interpretation of instantaneous growth, which has been classically used^[112–114] would be more convenient to describe the process assuming that new nucleation sites are activated as the transformation progresses, probably ascribed to the boundary of the formed regions where new dislocations are formed to store the elastic energy and those dislocations are expected to act as heterogeneous nucleation sites.^[110,113] In fact, reported slow growth rates extracted from kinetic analysis could be an artifact from imposing an inappropriate kinetic model such as KJMA.

7. Conclusions

KJMA theory is broadly used to interpret the kinetics of transformation in solid state in many different cases. However, a considerable number of them are beyond the applicability conditions. Understanding the restrictions allows us to interpret whether a physical meaning of the Avrami exponent is straightforward or not.

Even for those ideal processes following KJMA theory, determination of experimental parameters, particularly the induction time, is critical to obtain the correct Avrami exponent.

Taking into account an Arrhenius-like temperature dependence for the frequency factors, a direct extension to nonisothermal regimes works well for processes with Avrami exponent close to 1. For processes with a small temperature span, assuming an average frequency factor may lead to fair local values of n at low transformed fractions.

Despite decelerated growth processes, such as diffusion controlled one, are out of the KJMA theory and lead to overgrowth artifact, our simulations show that deviations are small and KJMA theory is a fairly good approximation to describe diffusion controlled growth processes.

In addition, some strategies for recovering parameters with physical meaning from KJMA analyses are proposed. Finally,

when growth process is not registrable, interpretation of the data in the frame of an instantaneous growth approximation allows us to analyze the nucleation rate.

Acknowledgements

This work was supported by AEI/FEDER-UE (Projects US-1260179 and P18-RT-746) and the PAI of the Regional Government of Andalucía. VI-PPUS from University of Seville is also acknowledged.

Conflict of Interest

The authors declare no conflict of interest.

Keywords

Avrami exponent, kinetics, KJMA theory, JMAK theory, JMA theory, solid-state transformations

Received: October 13, 2021

Revised: February 3, 2022

Published online:

- [1] A. N. Kolmogorov, *Bull. Acad. Sci. USSR, Phys. Ser.* **1937**, 1, 355; *Selected Works of A. N. Kolmogorov* (Ed: A. N. Shirayev), Vol. 2, Kluwer, Dordrecht **1992**, p. 188, English translation.
- [2] W. A. Johnson, R. F. Mehl, *Trans. Am. Inst. Mining Met. Engrs.* **1939**, 135, 416.
- [3] M. Avrami, *J. Chem. Phys.* **1941**, 9, 177.
- [4] A. A. Burbelko, E. Frás, W. Kapturkiewicz, *Mater. Sci. Eng., A* **2005**, 413, 429.
- [5] D. W. Henderson, *J. Non-Cryst. Solids* **1979**, 30, 301.
- [6] H. Yinnon, D. R. Uhlmann, *J. Non-Cryst. Solids* **1983**, 54, 253.
- [7] M. Fanfoni, M. Tomellini, *Il Nuovo Cimento D* **1998**, 20, 1171.
- [8] M. C. Weinberg, *J. Non-Cryst. Solids* **1999**, 255, 1.
- [9] M. T. Clavaguera-Mora, N. Clavaguera, D. Crespo, T. Pradell, *Prog. Mater. Sci.* **2002**, 47, 559.
- [10] A. D. Lueking, C. Y. Wang, S. Sircar, C. Malencia, J. Li, *Dalton Trans.* **2016**, 45, 4242.
- [11] F. S. Yang, Y. Zhang, F. Ciucci, Z. Wu, S. Wang, Y. Wang, Z. X. Zhang, *J. Alloys Compd.* **2018**, 741, 610.
- [12] N. A. Oladoja, *Desal. Water Treat.* **2016**, 57, 15813.
- [13] E. Lorente, J. A. Peña, J. Herguido, *Int. J. Hydrogen Energy* **2008**, 33, 615.
- [14] R. Serna-Guerrero, A. Sayari, *Chem. Eng. J.* **2010**, 161, 182.
- [15] I. Karsaj, J. D. Humphrey, *Biorheology* **2009**, 46, 509.
- [16] L. Benedini, D. Placente, J. Ruso, P. Messina, *Mater. Sci. Eng. C-Mater. Biol. Appl.* **2019**, 99, 180.
- [17] M. Morales-González, J. A. González-Joa, L. E. Bergues-Cabrales, A. E. Bergues-Pupo, B. Schneider, S. Kondakci, H. M. Camué-Ciria, J. Bory-Reyes, M. Verdecia-Jarque, M. A. O'Farril-Mateus, T. Rubio-González, S. C. Acosta-Brooks, J. L. Hernández-Cáceres, G. V. Sierra-González, *BMC Cancer* **2017**, 17, 174.
- [18] A. G. Hirsh, R. J. Williams, P. Mehl, *Exp. Gerontol.* **1994**, 29, 197.
- [19] G. Korniss, T. Caraco, *J. Theor. Biol.* **2005**, 233, 137.
- [20] A. Bawiec, T. Garbowski, K. Paweska, K. Pulikowski, *Water Air Soil Pollut.* **2019**, 230, 17.
- [21] T. H. Tran, A. Govin, R. Guyonnet, P. Grosseau, C. Lors, D. Damidot, O. Devés, B. Ruot, *Int. Biodeterior. Biodegrad.* **2013**, 79, 73.
- [22] Y. Nagano, K. L. Ode, *Phys. Biol.* **2014**, 11, 046008.

- [23] A. Baker, B. Audit, S. C. H. Yang, J. Bechloef, A. Arneodo, *Phys. Rev. Lett.* **2012**, *108*, 268101.
- [24] P. L. Ralph, G. Coop, *Am. Nat.* **2015**, *186*, S5.
- [25] L. O'Malley, J. Basham, J. A. Yasi, G. Korniss, A. Allstadt, T. Caraco, *Theor. Popul. Biol.* **2006**, *70*, 464.
- [26] B. T. Ho, D. C. Joyce, B. R. Bhandari, *Food Chem.* **2011**, *129*, 259.
- [27] C. Walters, L. M. Wheeler, J. M. Grotenhuis, *Seed Sci. Res.* **2005**, *15*, 1.
- [28] J. V. Santacatalina, J. V. García-Pérez, E. Corona-Jiménez, J. Benedito, *J. Food Res. Int.* **2011**, *44*, 146.
- [29] S. S. Hubbes, W. Danzl, P. Foerst, *LWT-Food Sci. Tech.* **2018**, *93*, 189.
- [30] S. S. Narine, K. L. Humphrey, L. Bouzidi, *J. Am. Oil Chem. Soc.* **2006**, *83*, 913.
- [31] M. Ausloos, F. Petroni, *Physica A-Stat. Mech. Appl.* **2009**, *388*, 4438.
- [32] A. Korobov, *J. Math. Chem.* **1998**, *24*, 261.
- [33] M. Tomellini, M. Fanfoni, *Eur. Phys. J.* **2003**, *B34*, 331.
- [34] B. J. Kooi, *Phys. Rev. B* **2006**, *73*, 054103.
- [35] J. Burke, in *The Kinetics of Phase Transformations in Metals*, Pergamon Press, Oxford, UK **1965**.
- [36] J. Christian, in *The Theory of Transformations in Metals and Alloys*, Pergamon Elsevier Science, Oxford, UK **2002**.
- [37] S. Vyazovkin, A. K. Burnham, J. M. Criado, L. A. Pérez-Maqueda, C. Popescu, N. Sbirrazzuoli, *Thermochim. Acta* **2011**, *520*, 1.
- [38] M. Tomellini, M. Fanfoni, *Physica A-Stat. Mech. Appl.* **2004**, *333*, 65.
- [39] M. Tomellini, *J. Mater. Sci.* **2013**, *48*, 5653.
- [40] M. J. Starink, *J. Mater. Sci.* **2001**, *36*, 4433.
- [41] J. B. Austin, R. L. Rickett, *Trans. Am. Inst. Mining Met. Eng.* **1939**, *135*, 396.
- [42] T. Tagami, S. I. Tanaka, *J. Mater. Sci.* **1999**, *4*, 355.
- [43] A. Calka, A. P. Radlinski, *J. Mater. Res.* **1988**, *3*, 59.
- [44] L. K. Varga, E. Bakos, L. F. Kiss, I. Bakonyi, *Mater. Sci. Eng. A* **1994**, *179*, 567.
- [45] C. F. Conde, A. Conde, *Mater. Lett.* **1994**, *21*, 409.
- [46] V. Ocelík, K. Csach, A. Kasardová, J. Miškuf, P. Švec, K. Křištiaková, I. Mat'ko, *Scr. Mater.* **1996**, *35*, 1301.
- [47] J. S. Blázquez, C. F. Conde, A. Conde, *Appl. Phys. A* **2003**, *76*, 571.
- [48] E. Illekova, *Thermochim. Acta* **2002**, *387*, 47.
- [49] M. E. McHenry, F. Johnson, H. Okumura, T. Ohkubo, V. R. V. Ramanan, D. E. Laughlin, *Scr. Mater.* **2003**, *48*, 881.
- [50] A. Danzig, N. Mattern, *Phys. Status Solidi A* **1995**, *147*, 335.
- [51] P. Bruna, D. Crespo, R. González-Cinca, E. Pineda, *J. Appl. Phys.* **2006**, *100*, 054907.
- [52] M. Jovanovic, *J. Less Common Met.* **1971**, *25*, 237.
- [53] R. W. Knights, P. Wilkes, *Met. Alloys Trans.* **1973**, *4*, 2389.
- [54] J. C. Guía-Tello, C. G. Garay-Reyes, M. A. Ruiz-Esparza-Rodríguez, L. J. García-Hernández, J. Aguilar-Santillán, I. Estrada-Guel, R. Martínez-Sánchez, *Mater. Chem. Phys.* **2021**, *271*, 124927.
- [55] N. Kherrouba, Br. Mehdi, R. Kouba, R. Badji, C. A. Dekik, Y. T. Tounsi, *Mater. Chem. Phys.* **2021**, *266*, 124574.
- [56] G. Laplanche, S. Berglund, C. Reinhart, A. Kostka, F. Fox, E. P. George, *Acta Mater.* **2018**, *161*, 338.
- [57] C. Capdevila, M. K. Miller, J. Chao, *Acta Mater.* **2012**, *60*, 4673.
- [58] W. Sha, *Phys. Status Solidi A* **2005**, *202*, 1903.
- [59] T. Nagase, I. Yamauchi, I. Ohnaka, *J. Alloys Compd.* **2001**, *316*, 212.
- [60] Z. Xiang, T. Wang, S. Ma, L. Qian, Z. Luo, Y. Song, H. Yan, W. Lu, *J. Alloys Compd.* **2018**, *741*, 951.
- [61] B. S. Murty, D. H. Ping, M. Ohnuma, K. Hono, *Acta Mater.* **2001**, *49*, 3453.
- [62] M. Tomellini, *Comput. Mater. Sci.* **2011**, *50*, 2371.
- [63] T. Pradell, D. Crespo, N. Clavaguera, M. T. Clavaguera-Mora, *J. Phys. Cond. Matter* **1998**, *3833*.
- [64] T. Ozawa, *Polymer* **1971**, *12*, 150.
- [65] M. L. Di Lorenzo, C. Silvestre, *Prog. Polym. Sci.* **1999**, *24*, 917.
- [66] J. Malek, *Thermochim. Acta* **1995**, *267*, 61.
- [67] K. Nakamura, T. Watanabe, K. Katayama, *J. Appl. Polymer Sci.* **1972**, *16*, 1077.
- [68] A. T. W. Kempen, F. Sommer, E. J. Mittemeijer, *J. Mater. Sci.* **2002**, *37*, 1321.
- [69] H. E. Kissinger, *Anal. Chem.* **1957**, *29*, 1702.
- [70] J. S. Blázquez, V. Franco, C. F. Conde, M. Millán, A. Conde, *J. Non-Cryst. Solids* **2008**, *354*, 3597.
- [71] J. S. Blázquez, M. Millán, C. F. Conde, A. Conde, *Phys. Status Solidi A* **2010**, *207*, 1148.
- [72] J. S. Blázquez, C. F. Conde, A. Conde, *Acta Mater.* **2005**, *53*, 2305.
- [73] J. S. Blázquez, J. M. Borrego, C. F. Conde, A. Conde, S. Lozano-Pérez, *J. Alloys Compd.* **2012**, *544*, 73.
- [74] J. S. Blázquez, C. F. Conde, A. Conde, *Int. J. Therm. Sci.* **2015**, *88*, 1.
- [75] J. S. Blázquez, J. J. Ipus, C. F. Conde, D. Cabrera, V. Franco, A. Conde, *J. Alloys Compd.* **2014**, *615*, S213.
- [76] A. F. Manchón-Gordón, J. J. Ipus, J. S. Blázquez, C. F. Conde, A. Conde, P. Svec Sr., *J. Alloys Compd.* **2020**, *825*, 154021.
- [77] A. F. Manchón-Gordón, P. Svec, J. J. Ipus, M. Kowalczyk, J. S. Blázquez, C. F. Conde, A. Conde, P. Svec Sr., T. Kulik, *Metall. Mater. Trans. A* **2020**, *51*, 1395.
- [78] A. F. Manchón-Gordón, J. S. Blázquez, C. F. Conde, A. Conde, *J. Alloys Compd.* **2016**, *675*, 81.
- [79] M. J. Starink, *J. Mater. Sci.* **1997**, *32*, 4061.
- [80] C. Suryanarayana, *Prog. Mater. Sci.* **2001**, *46*, 1.
- [81] P. Baláž, M. Achimovičová, M. Baláž, P. Billik, Z. Cherkezova-Zheleva, J. M. Criado, F. Delogu, E. Dutková, E. Gaffet, F. J. Gotor, R. Kumar, I. Mitov, T. Rojac, Mamoru Senna, A. Streletskii, K. Wieczorek-Ciurow, *Chem. Soc. Rev.* **2013**, *42*, 7571.
- [82] N. Yermakov, A. Y. Yurchikov, V. A. Barinov, *Fiz. Met. Metall.* **1981**, *52*, 1184.
- [83] C. C. Koch, O. B. Cabin, C. G. Mckamey, J. O. Scarbrough, *Appl. Phys. Lett.* **1983**, *43*, 1017.
- [84] J. S. Blázquez, J. J. Ipus, L. M. Moreno-Ramírez, J. M. Álvarez-Gómez, D. Sánchez-Jiménez, S. Lozano-Pérez, V. Franco, A. Conde, *J. Mater. Sci.* **2017**, *52*, 11834.
- [85] J. S. Blázquez, J. J. Ipus, A. Conde, *Scr. Mater.* **2017**, *130*, 260.
- [86] F. Manchón-Gordón, J. J. Ipus, J. S. Blázquez, C. F. Conde, A. Conde, *J. Non-Cryst. Solids* **2018**, *494*, 78.
- [87] F. Delogu, G. Cocco, *J. Alloys Compd.* **2007**, *436*, 233.
- [88] F. Delogu, C. Deidda, G. Mulas, L. Schiffrini, G. Cocco, *J. Mater. Sci.* **2004**, *39*, 5121.
- [89] F. Delogu, L. Takacs, *Acta Mater.* **2014**, *80*, 435.
- [90] H. Moumeni, S. Alleg, J. M. Greneche, *J. Alloys Compd.* **2006**, *419*, 140.
- [91] S. Louidi, F. Z. Bentayeb, J. J. Sunol, L. Escoda, *J. Alloy. Compd.* **2010**, *493*, 110.
- [92] N. Loudjani, N. Bensebaa, S. Alleg, C. Djebbari, J. M. Greneche, *Phys. Status Solidi A* **2011**, *208*, 2124.
- [93] Y. P. Shen, H. H. Hng, J. T. Oh, *Mater. Lett.* **2004**, *58*, 2824.
- [94] R. S. Lei, M. P. Wang, H. P. Wang, S. Q. Xu, *Character* **2016**, *118*, 324.
- [95] Y. Konishi, K. Kadota, Y. Tozuka, A. Shimosaka, Y. Shirakawa, *Powder Technol.* **2016**, *301*, 220.
- [96] S. Alleg, A. Hamouda, S. Azzaza, R. Bensalem, J. J. Sunol, J. M. Greneche, *Mater. Chem. Phys.* **2010**, *122*, 35.
- [97] M. S. El-Eskandarany, A. A. Bahgat, N. S. Gomaa, N. A. Eissa, *J. Alloys Compd.* **1999**, *290*, 181.
- [98] J. S. Blázquez, A. F. Manchón-Gordón, J. J. Ipus, C. F. Conde, A. Conde, *Metals* **2018**, *8*, 450.
- [99] W. Lu, L. Yang, B. Yan, W. H. Huang, *Phys. Status Solidi A* **2005**, *202*, 1733.
- [100] B. Chen, S. Yang, X. Liu, B. Yan, W. Lu, *J. Alloys Compd.* **2008**, *448*, 234.
- [101] J. S. Blázquez, M. Millán, C. F. Conde, A. Conde, *J. Alloys Compd.* **2010**, *505*, 91.

- [102] J. S. Blázquez, C. F. Conde, A. Conde, *J. Non-Cryst. Solids* **2011**, 357, 2833.
- [103] D. Koistinen, R. Marburger, *Acta Metall.* **1959**, 7, 59.
- [104] C. Liu, Y. Shao, J. Chen, Y. C. Liu, *Appl. Phys. A* **2016**, 122, 715.
- [105] A. F. Manchón-Gordón, R. López-Martín, J. J. Ipus, J. S. Blázquez, P. Svec Sr, C. F. Conde, A. Conde, *Metals* **2021**, 11, 849.
- [106] J. S. Blázquez, C. F. Conde, A. Conde, *J. Non-Cryst. Solids* **2001**, 287, 187.
- [107] F. J. Romero-Landa, J. M. Martín-Olalla, J. S. Blázquez, M. C. Gallardo, D. Soto Serra, E. Vives, A. Planes, *J. Alloys Compd.* **2021**, 887, 161395.
- [108] M. C. Gallardo, J. Jiménez, J. del Cerro, *Rev. Sci. Instrum.* **1995**, 66, 5288.
- [109] F. J. Romero, M. C. Gallardo, J. M. Martín-Olalla, J. del Cerro, *Thermochim. Acta* **2021**, 706, 179053.
- [110] M. Suezawa, H. E. Cook, *Acta Metall.* **1980**, 28, 423.
- [111] F. J. Pérez-Reche, E. Vives, L. Mañosa, A. Planes, *Phys. Rev. Lett.* **2001**, 87, 195701.
- [112] A. R. Entwisle, *Metall. Trans.* **1971**, 2, 2395.
- [113] S. M. C. van Bohemen, J. Sietsma, M. J. M. Hermans, I. M. Richardson, *Acta Mater.* **2003**, 51, 4183.
- [114] J. R. C. Guimaraes, P. R. Rios, *Metall. Mater. Trans. A* **2012**, 44, 2.



Javier Sebastián Blázquez Gámez is a full professor at the Department Physics of Condensed Matter, Faculty of Physics, University of Seville. He is ascribed to the Non-Crystalline Solids Research Group (FQM-121 Research Group at the University of Seville). His fields of interest include metastable soft magnetic materials, crystallization kinetics, and magnetocaloric effect.



Francisco Javier Romero Landa is an associate professor at the Department Physics of Condensed Matter, Faculty of Physics, University of Seville. He is ascribed to the Thermal and Dielectric Properties of Solids Research Group (FQM-130 Research Group at the University of Seville). His fields of interest include phase transitions, metastability, avalanches, calorimetry, and shape-memory alloys.



Clara Francisca Conde Amiano is a full professor at the Department Physics of Condensed Matter, Faculty of Physics, University of Seville. She is the head of the Non-Crystalline Solids Research Group (FQM-121 Research Group at the University of Seville). Her fields of interest include metastable soft magnetic materials, crystallization kinetics, and magnetocaloric effect.



Alejandro Conde Amiano is an emeritus professor at the Department Physics of Condensed Matter, Faculty of Physics, University of Seville. He is ascribed to the Non-Crystalline Solids Research Group (FQM-121 Research Group at the University of Seville). His fields of interest include metastable soft magnetic materials, crystallization kinetics, magnetocaloric effect.